NANOSTRUCTURE FABRICATION AND PATTERNING FOR USE IN CHEMICAL SEPARATIONS AND SENSORS

By

SHUFANG YU

A DISSERTATION PRESENTED TO THE GRADUATE SCHOOL
OF THE UNIVERSITY OF FLORIDA IN PARTIAL FULFILLMENT
OF THE REQUIREMENTS FOR THE DEGREE OF
DOCTOR OF PHILOSOPHY

UNIVERSITY OF FLORIDA

2003

To my family, for their continued support and love.

ACKNOWLEDGMENTS

During my years at graduate school, many individuals have been there to advise, help and encourage me along the way

I would like to thank Dr Charles R. Martin for his guidance, assistance and support throughout my graduate career I enjoyed working in his group very much. In addition, I appreciate the independence and patience that Dr Martin affords all of his students.

For sharing the experience of graduate school I would like to thank all the past and present members of the Martin group for being supportive. Sangbok Lee, Damian Odom, Marc Wirtz, and Punit Kohli gave me insightful advice on my project. Sangbok Lee and Munsik Kang showed great patience in training me in electroless gold deposition. Myungchan Kang and Nuchao Li are creative scientists who know the value of collaboration. In particular I would like to thank Elizabeth Heins and Damian Odom for their help in proofreading this dissertation. I am truly grateful to have had the opportunity to work with all of these talented people and will miss them very much in the future.

For encouragement and help throughout my journey before and during graduate school, I would like to thank my family and my friends. My family provided unflagging moral support throughout my graduate career My beloved one–Qingguo Song–has always been there to encourage and assist me. My parents Qincai Yu and Quanmei Zheng, my sister Yufang Yu and my brothers Zuzhong Yu and Zucheng Yu have been a constant source of love and support I would like to thank my friends Hongxin Zhang

Bo Pang, Hongbong Zhang, Guangyu Sun, Li Li and Qian Li for reminding me that outside of graduate school life continues and I need to join the outside world once again. I owe many thanks to all of them.

TABLE OF CONTENTS

Page

ACKNOWLEDGMENTS ... iii

LIST OF TABLES ... vii

LIST OF FIGURES ... viii

ABSTRACT ... xi

CHAPTER

1 INTRODUCTION AND BACKGROUND ... 1

Membrane-based Template Synthesis ... 2
Templates Used in Template Synthesis ... 2
Synthetic Strategies in Template Synthesis ... 4
Applications of Gold Nanotube and Nanowire Membranes ... 11
Protein Separations with Membrane Ultrafiltration Techniques ... 14
Plasma Based Etching ... 16
Dissertation Overview ... 17

2 PROTEIN TRANSPORT IN ENGINEERED GOLD NANOTUBE MEMBRANES ... 20

Introduction ... 20
Experimental ... 23
Materials ... 23
Membrane Preparation ... 23
Protein Transport Experiments ... 24
Applied transmembrane pressure ... 24
Applied transmembrane potential ... 26
Results and Discussion ... 28
Applied Transmembrane Pressure ... 29
Applied Transmembrane Potential ... 33
Single-protein transport experiments ... 33
Lys/BSA two-protein transport experiments ... 37
CA/Hb two-protein transport experiments ... 41
Hb/BSA two-protein transport experiments ... 42
Conclusions ... 45

3 NANO WHEAT FIELDS PREPARD BY PLASMA-ETCHING GOLD NANOWIRE-CONTAINING MEMBRANES ... 47

Introduction ... 47
Experimental ... 48
Results and Discussion ... 49
Conclusions ... 55

4 CONTROLLABLE AND ADDRESSABLE GLASS NANOWELLS FROM PLASMA ETCHING ... 56

Introduction ... 56
Experimental ... 57
Materials ... 57
Preparation of the Nanopore Alumina Membrane ... 59
Fabrication of Nanowells ... 60
Atomic Force Microscopy (AFM) ... 61
Silica Nanoparticle Synthesis and Characterization ... 62
Chemical Modification Inside and Outside of the Nanowells ... 63
Selective Attachment of Nanoparticles ... 65
Silica nanoparticle attachment ... 65
Polystyrene nanoparticle attachment ... 67
Results and Discussion ... 67
Depth of the Etched Nanowells ... 67
Selective Attachment of Nanoparticles ... 70
Silica nanoparticle attachment ... 70
Polystyrene nanoparticle attachment ... 73
Friction Measurements with AFM ... 74
Conclusions ... 79

5 CONCLUSIONS ... 81

LIST OF REFERENCES ... 85

BIOGRAPHICAL SKETCH ... 93

LIST OF TABLES

Table		page
2-1	Concentration of proteins in the permeate and transport selectivity coefficients for two-protein (Lys/BSA) permeation experiments.	32
2-2	Concentration of proteins in the permeate and transport selectivity coefficients for two-protein (LGA/BSA) permeation experiments.	32
2-3	Comparison of average Lys flux values obtained from two-protein (Lys/BSA) and single-protein (Lys) transport experiments.	39
2-4	Transmembrane potential required to shut down BSA transport in membranes having nanotubes with the indicated diameters.	40
2-5	Comparison of diffusive and electrophoretic fluxes of BSA and Hb for two-protein permeation experiments at pH = 4.9 (isoelectric point of BSA) and pH = 7.0 (isoelectric point of Hb)	44

LIST OF FIGURES

Figure		page
1-1	Scanning electron micrographs of the membrane surfaces	3
1-2	Schematic representations of the concept of forming nanotubes in the pores of a template membrane	5
1-3	Schematic diagram of the Au electroless plating procedure used to deposit gold in the pores of the polycarbonate template membrane.	8
1-4	Schematic illustrations of Au nanotubes obtained from electroless gold plating, which yielding structures running the complete thickness of the template membrane	9
1-5	Variation of the nanotube effective inside diameter with plating time.	11
2-1	Schematic of the transport cell with applied pressure.	25
2-2	Schematic of the four-compartment transport cell.	27
2-3	Plots of moles transported vs. time for Lys diffusion (no applied pressure) across ID = 23-nm Au nanotube membranes.	29
2-4	Plots of moles transported vs. time for Lys (upper) and BSA (lower) across an ID = 40-nm Au nanotube membrane	30
2-5	HPLC data for two-protein (Lys/BSA) permeation experiments.	31
2-6	HPLC data for two-protein (LGA/BSA) permeation experiments	33
2-7	Plot of nmoles of Lys transported vs time in a membrane with 40 nm ID nanotubes with and without an applied transmembrane potential of +6 V	34
2-8	Plots of flux vs. applied transmembrane potential for Lys and BSA.	35
2-9	Lys concentration vs time in the permeate and feed solutions during a permeation experiment.	36
2-10	Selectivity and flux vs. nanotube ID for the Lys/BSA separation.	38
2-11	Selectivity and flux vs nanotube ID for the CA/Hb separation.	41

2-12 Diffusive and electrophoretic fluxes of BSA and Hb for two-protein permeation experiments at different pH under the applied potential ... 43

3-1 Scanning electron micrographs (SEMs) of the template membrane before (A) and after (B) electroless deposition of the Au nanowires ... 49

3-2 SEM image of the surface of the Scotch tape after using the tape to remove a Au surface film. ... 50

3-3 SEMs of the surfaces of membranes that were O_2-plasma etched for 5 (A), 10 (B), 30 (C), 60 (D) and 120 (E) seconds ... 51

3-4 Plot of length of the plasma-exposed portion of the Au nanowires vs. plasma etching time ... 52

3-5 SEMs of the surfaces of membranes that were O_2-plasma etched for 180 (A) 240 (B), and 400 (C) seconds ... 53

4-1 Structures of silanes used for modification. ... 58

4-2 Scanning electron micrographs of alumina membrane. ... 59

4-3 Glass etching process by argon plasma. ... 61

4-4 TEM image of the silica nanoparticles. ... 62

4-5 Different modification inside and outside of the nanowells ... 63

4-6 Nanowell etching process from Au/Pd sputtered glass. ... 64

4-7 Procedure of attaching silica nanoparticles into the nanowells and the control experiments ... 66

4-8 500 nm x 500 nm AFM images of etched glass at different etching time ... 68

4-9 Depth measurements of the nanowells. ... 69

4-10 AFM image of the resulted nanowells etched from Au/Pd sputtered glass ... 70

4-11 Selective attachment of silica nanoparticles into nanowells ... 71

4-12 AFM images of control experiments by neglecting one of the silanes ... 72

4-13 AFM image of polystyrene nanoparticle selective attachment into the nanowells. 74

4-14 Plots of frictional signal vs. lateral displacements during 250 nm trace/retrace cycles along a single scan line at 1000 nm/s. ... 75

4-15 Friction forces as a function of applied loads for modified surfaces with different chemistry 75

4-16 AFM height and friction images when NH_2–terminated molecules are outside the nanowells and CH_3–terminated ones are inside the nanowells. 77

4-17 The corresponded height and friction force measurements to Figure 4-16. 78

Abstract of Dissertation Presented to the Graduate School
of the University of Florida in Partial Fulfillment of the
Requirements for the Degree of Doctor of Philosophy

NANOSTRUCTURE FABRICATION AND PATTERNING FOR USE IN CHEMICAL SEPARATIONS AND SENSORS

By

Shufang Yu

December 2003

Chair: Charles R. Martin
Major Department: Chemistry

The goals of this research are to make nanostructures with controlled dimensions and to investigate potential applications in chemical separations and sensors. There are three parts involved in this work. The first part is engineered gold nanotube membranes and their applications in protein separations. The membranes have narrow pore size distribution, high selectivity, and they are relatively easily modified to prevent protein adsorption. Because of the low transport rate or throughput through the membrane, two types of driving forces were applied to increase transport flux--application of a transmembrane pressure or a transmembrane potential difference. Size-sieving effect, charge effect and pH effect have been investigated.

The second part of this work is a method developed to increase the efficiency of nanowires as building blocks for supramolecular assembly. The low efficiency results from some recessed nanowires within the template membrane. Oxygen plasma etching has been used to remove part of the polymer template and leave the nanowire ends

exposed. By adjusting etching time, the length of the protruding nanowires can be controlled. Besides high efficiency as building blocks, these protruding nanowires can be used to increase electrical contact between the nanowire containing membrane and a substrate metal surface.

In the third part of this work, highly ordered alumina membranes were used as masks to etch substrates such as glass to obtain arrays of nanowells. The depth of the nanowells can be controlled by varying the etch time. The inside and outside of the nanowells can be modified with different chemistries such as hydrophilic and hydrophobic functional groups. Friction measurements with the atomic force microscope have been conducted to obtain the friction difference between the different functional groups. The friction difference shows the interaction difference between the AFM tip and the terminal functional groups on the substrate. Since the inside and outside of the nanowells can be modified with different molecular linkers, desired chemical functional groups or nanoparticles can attach to either the inside or outside surfaces.

CHAPTER 1
INTRODUCTION AND BACKGROUND

Nanotechnology is revolutionizing the electronic, chemical and biotechnology fields.[1] In contrast with the top-down manufacturing strategy used in industry, nanotechnology involves a bottom-up alternative. By building up new products from molecules and nanostructures, similar to the strategies of Mother Nature, it is possible to construct complex nanoscale architectures. Many areas are expected to benefit from nanotechnology including the semiconductor industry, biomedical devices, energy storage, electronic devices, and chemical and biosensors.[2,3] Nanofabrication and nanopatterning are making it possible to develop diverse applications of nanostructured devices. Nanofabrication and nanopatterning refer to the tools and the techniques for changing the structures and the properties of matter at the nanoscale. One of the key elements in the successful development of these devices is the ability to control the dimensions of nanostructures.

This chapter is divided into five sections which provide the background information for this research. Section 1 reviews membrane-based template synthesis. This method, pioneered by the Martin group, is used in preparation of the nanostructured materials described in Chapters 2 and 3. Section 2 discusses applications of gold nanotube and nanowire membranes synthesized by electroless gold plating-based template synthesis. In section 3, protein separation with membrane ultrafiltration techniques is reviewed. Section 4 covers the plasma based etching technique which has

been used to control the dimensions of nanostructures in Chapters 3 and 4. Finally, section 5 is the dissertation overview.

Membrane-based Template Synthesis

In recent years, our group has pioneered a general method for preparation of nanomaterials called template synthesis.[4-6] Reviews of this method can be found elsewhere in the literature.[5-7,8] The method is termed "general" because nearly any chemical synthesis method used to prepare bulk materials can be adapted to synthesize nanomaterials. In the template method, the material of interest is deposited within the nanometer-sized pores of a host solid. The size and the shape of the nanomaterial depend on the dimensions of the nanocavities in the host template.

Templates Used in Template Synthesis

Membrane-based template synthesis entails deposition of desired materials within the pores of a nanopore membrane. The membranes employed in this research have cylindrical pores of uniform diameter. Each of these pores is viewed as sort of a beaker in which the desired material is synthesized. Because of the shape of the pores, a nanocylinder of the materials is deposited in each pore. Depending on the materials and the chemistry of the pore wall, this nanocylinder may be solid (nanowires) or hollow (nanotubes).

Different types of membranes are used as templates in membrane-based template synthesis. The most commonly used types are "track-etched" membranes and nanopore alumina membranes.[4,8] These membranes are characterized by cylindrical pores that extend through the entire thickness of the membrane. Figure 1-1 shows scanning electron micrographs of the surfaces of these membranes. The first type is called "track-etched" because these membranes are prepared via the "track-etch" two-step method.[9] In the

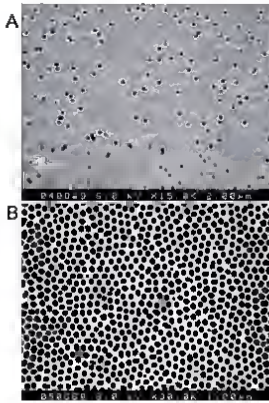

Figure 1-1 Scanning electron micrographs of the membrane surfaces (A) polycarbonate track-etched membrane, (B) alumina membrane

first step, thin plastic film such as polycarbonate or polyester is exposed to a beam of high energy nuclear fission fragment from a nuclear reactor, forming randomly distributed damage through the film. The number of tracks depends primarily on the amount of time that the film is exposed to the fission fragment beam. In the second step, the tracks are preferentially etched into uniform, cylindrical pores by a strong alkaline solution. The resulting membranes contain randomly distributed cylindrical pores of uniform diameter ranging from 20 μm to10 nm. A number of companies sell microporous and nanoporous membranes prepared by the track-etch method.

Another important type of template in membrane based template synthesis is the nanopore alumina membranes, prepared electrochemically from aluminum metal foil [10-16] The pores in these membranes are arranged in a regularly hexagonal lattice with a narrow pore-size distribution and high pore density (Figure 1-1B) [10-18] Membranes of this type are available commercially but with only three different pore diameters. However in our research group we make highly ordered alumina membranes with controllable thickness and pore size using a "two-step anodization" process.[19] At the beginning of the aluminum anodization, the pores in the nascent alumina film initiate at almost random positions Pore arrangement on the surface is disordered with a broad pore size distribution.[13] However, order and monodispersity of pore size increase with growth time as explained by the self-organized growth model.[14] After this initial anodization step, the alumina film obtained is dissolved away in an acidic solution. An ultrathin film of highly ordered alumina is left on the aluminum surface which acts as a template for the second oxidization step In this second anodization step, a densely packed hexagonal porous film is obtained. The anodizing voltage controls the pore size and pore density, whereas the thickness is determined by the anodization time.[11, 12] Therefore, by choosing the proper voltage, current, temperature and anodization time, the pore sizes and thickness of membranes can be controlled

Other material templates used for template synthesis include nanochannel array glass membranes,[20] zeolites,[21] and proteins.[22, 23]

Synthetic Strategies in Template Synthesis

Membrane-based template synthesis has been used to prepare nanomaterials composed of electronically conductive polymers,[24-33] metals,[34-45] semiconductors,[46, 47] carbons and other materials.[48, 49] The synthetic strategies adapted from preparation of

bulk materials including chemical vapor deposition,[49-51] electrochemical[39 52 53] and electroless deposition,[43 54] chemical[48] and electrochemical polymerization,[55] and sol-gel chemistry.[46, 56] Figure 1-2 shows the basic idea of template synthesis via different chemistry strategies. Special attention will be given to electroless deposition since this is the chemistry used for preparation of the nanomaterials in Chapters 2 and 3.

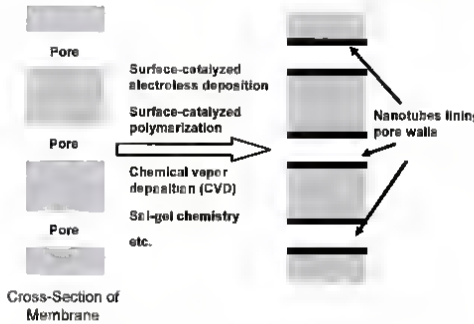

Figure 1-2. Schematic representations of the concept of forming nanotubes in the pores of a template membrane.

Chemical vapor deposition (CVD). CVD is commonly used to prepare carbon nanomaterials. Our group[49, 57] and others[58, 59] have synthesized carbon nanotubes within the porous alumina template membranes using CVD. This involves placing an alumina membrane in a high-temperature furnace (ca. 700 ° C) and passing a gas such as ethane, propene or ethylene through the membrane. Thermal decomposition of the gas occurs on the pore walls, resulting in the deposition of carbon nanotubes within the pores. High

surface area microporous carbon with long-range order has also been synthesized by using zeolite Y as a template with propylene CVD.[60] Besides carbon nanostructures, other nanomaterials have been obtained by CVD. For example, the Martin group has used a CVD method to coat an ensemble of gold nanotubes with concentric TiS_2 outer nanotubes.[61]

Sol-gel chemistry. Sol-gel chemistry is a general and powerful approach for the preparation of inorganic materials. This method involves hydrolysis of a solution of a precursor molecule to obtain a suspension of colloidal particles (the sol) and then a gel composed of aggregated sol particles. This chemistry has been used to prepare semiconductor nanofibers and nanotubes including TiO_2, WO_3 and ZnO within the pores of an alumina template.[62,63] Recently, our group synthesized silica nanotubes using sol-gel chemistry in the alumina templates and used these nanotubes in bioseparation and biocatalysis.[64] Sol-gel chemistry can also be used to make composite materials. Recently, the Aida group in Japan successfully fabricated a novel composite material consisting of polypyrrole nanofibers segregated and insulated by hexagonal silicate channels by using a sol-gel-based template polymerization of a pyrrole-containing surfactant monomer.[65] Using sol-gel chemistry on indium tin oxide (ITO) glass, different silica sol-gel were prepared and used as the host matrix for the electrochemical growth of polythiophene conductive polymer.[24]

Chemical and electrochemical polymerization. Chemical polymerization of nanowires or nanotubes can be accomplished by immersing the template membrane into a solution of the monomer and a polymerization reagent. In some cases, the polymer preferentially nucleates and grows on the pore walls, resulting in nanotubes of shorter

time and fibers at longer time. Chemical and electrochemical template synthesis has been used to prepare a variety of conductive polymers[26, 30, 53, 66-68] and electronically insulating plastics.[48]

Electrochemical metal deposition In this method, one face of the porous membrane is first coated with a metal film through sputtering or thermal evaporation. After that, the metal film is used as a cathode to electrodeposit one material within the pores of the membrane. This method has been used to prepare a variety of metal nanowires including copper, platinum, gold, silver and nickel in templates such as polycarbonate and alumina membranes.[34-39, 69]

Recently metallic barcodes (complex striping patterns) have been prepared by sequential electrochemical deposition of metal ions into templates with uniformly sized pores followed by barcode release by dissolving away the templates.[70] A silver film deposited on the back side of an alumina membrane serves as the working electrode for reduction of metal ions from solution. The structure of the barcodes is determined by the membrane pore diameter, the sequence of the metal ions introduced into solution and the charge passed in each step, dictating the stripe length. Seven different metals (Pt, Pd, Ni, Co, Ag, Cu, and Au) have been incorporated in segments ranging from 10 nm to several microns.

Electroless deposition. Electroless deposition involves the use of a chemical reducing agent to plate a metal from a solution onto a surface. Unlike electrochemical deposition, a conductive surface is not necessary. The key requirement of electroless deposition is arrangement of the chemistry such that the kinetics of homogeneous

electron transfer from the reducing agent to the metal ions is slow. This is essential because otherwise the metal ions would simply be reduced in the bulk solution. In

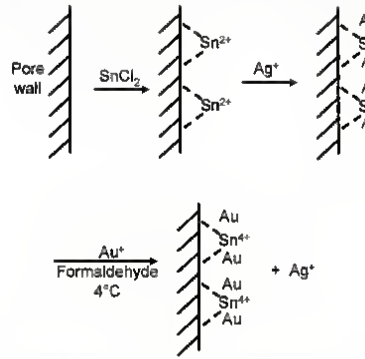

Figure 1-3. Schematic diagram of the Au electroless plating procedure used to deposit gold in the pores of the polycarbonate template membrane

electroless deposition, a catalyst needs to be coated onto the pore walls so that reduction of the metal ions occurs only at the pore surfaces. The electroless deposition chemistry I used to prepare gold nanowires and nanotubes is shown schematically in Figure 1-3. The polycarbonate membrane is first exposed to a sensitizer (Sn^{2+}). This is accomplished by simply immersing the membrane for 45 minutes into a solution that is 0.026 M in $SnCl_2$ and 0.07 M in trifluoroacetic acid in 50/50 (v/v) methanol/water. The sensitizer binds to the pore walls and membrane surfaces via complexation with the surface amine, carbonyl and hydroxyl groups.[43] After sensitization, the membrane is rinsed with methanol and then immersed into an aqueous solution of ammoniac silver nitrate (0.029 M $Ag(NH_3)_2^+$)

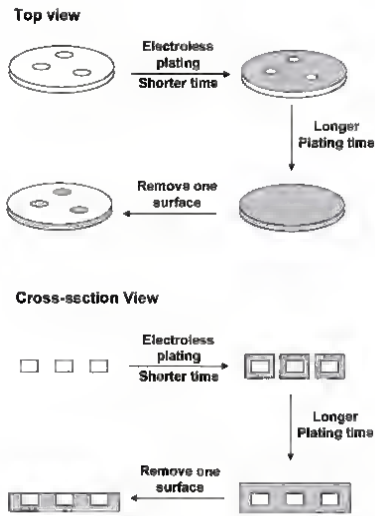

Figure 1-4 Schematic illustrations of Au nanotubes obtained from electroless gold plating, which yielding structures running the complete thickness of the template membrane.

for 5 minutes. A redox reaction occurs in which the surface-bound tin (II) is oxidized to tin (IV) and the Ag^+ is reduced to elemental Ag. As a result, the pore walls and membrane faces become coated with nanoscopic Ag particles. The membrane is again rinsed with methanol. The silver-coated membrane is then immersed into a gold plating bath that is 7.9×10^{-3} M in $Na_3Au(SO_3)_2$, 0.127 M in Na_2SO_3, and 0.625 M in

formaldehyde at 4°C. Au galvanically displaces the Ag particles because the reduction potential of Au is more positive than that of Ag. As a result, the pore walls and surfaces become coated with Au particles. These particles are excellent catalytic sites for the oxidation of the formaldehyde and the concurrent reduction of Au (I) to Au (0).[43] Without a catalyst, the kinetics of electron transfer from the reducing agent (formaldehyde) to Au(I) is slow, therefore, gold plating continues on the gold particles instead of in the bulk solution. The reaction can be represented as follows:

$$2Au(I) + HCHO + 3OH^- \rightarrow HCOO^- + 2H_2O + 2Au(0)$$

This method yields the Au nanowires or nanotubes within the pores plus Au surface layers on both faces of the membrane. These structures run through the complete thickness of the template membrane (Figure 1-4). By controlling the plating time, the inside diameter of the nanotubes can be varied because the thickness of both the Au surface films and nanotube walls increases with plating time. The inside diameter (ID) was measured using a gas transport method described elsewhere.[44, 71, 77] Briefly, the tube-containing membrane is placed in a gas-permeation cell, and the upper and lower half cells are evacuated. The upper half-cell is then pressurized, typically to 20 psi with H_2, and the pressure-time transient associate with leakage of H_2 through the nanotubes is measured using a pressure transducer in the lower half-cell. The pressure-time transient is converted to gas flux (Q, mol s^{-1}) which is related to the radius of the nanotubes (r, cm) via[73, 76]

$$Q = 4/3(2\pi/MRT)^{1/2}(nr^3 \Delta P/l) \qquad (1)$$

where ΔP is the pressure difference across the membrane (dyne cm^{-2}), M is the molecular weight of the gas, R is the gas constant (erg K^{-1} mol^{-1}), n is the number of the nanotubes

in the membrane sample l is the membrane thickness (cm) and T is the temperature

In using equation (1) we assume (i) that we know the number of nanotubes (n) in the membrane sample, (ii) that the nanotubes have a constant inside diameter down their entire length, and (iii) that the mechanism of gas transport through the membrane is Knudsen diffusion in the nanotubes. The number of nanotubes can be obtained from pore density and membrane area.

Figure 1-5 shows the variation of the nanotube effective inside diameter with plating time. Shorter deposition time yielded hollow nanotubes; at very long deposition times tubes fill in to make solid nanowires [78]

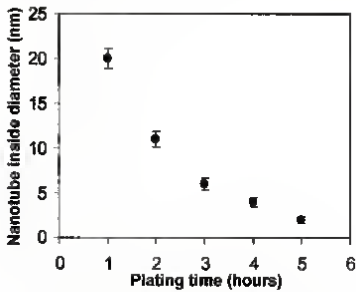

Figure 1-5 Variation of the nanotube effective inside diameter with plating time

Applications of Gold Nanotube and Nanowire Membranes

By controlling the gold plating time, the inside diameter (ID) of the nanotubes can be varied, even as low as 1 nm in diameter [72] As a result, these membranes can be used

in a simple membrane-permeation experiment to cleanly separate small molecules on the basis of molecular size [72]. By chemisorbing appropriate thiols to the Au nanopore walls based on the well-known gold-thiol chemistry, the Au nanopore membranes can be made to preferentially transport cations vs anions and hydrophobic vs hydrophilic molecules.[44, 71, 73, 79] In addition, Au nanotube membranes are electronically conductive and can be charged electrostatically in an electrolyte solution.[44] This introduces ion-transport selectivity, allowing the Au nanotube membranes to be electromodulated between ideal-cation and ideal-anion transport states [44]. The more challenging concept of electromodulating neutral molecule transport across the Au nanotube membrane has also been investigated [80]. The system developed in the work is a hybrid between the thiol chemisorption route for introducing chemical transport selectivity and the electrostatic charging route for controlling ion-transport selectivity [80]. Thus, these Au nanotube membranes are ideal model systems for studying how pore size, chemistry, and charge affect transport selectivity of membranes.

An exciting application of gold nanowires can be found in electrochemistry. Nanoelectrode ensembles (NEEs) prepared by the template method offer lower detection limits than conventional macroscopic electrodes.[81, 82] The template method in conjuction with electroless gold plating chemistry allows for the preparation of gold nanodisks with diameters as small as 10 nm [43]. This was accomplished by plating for a period of 24 hours, which resulted in the deposition of solid Au nanowires into the pores of the polycarbonate membranes. Removal of the gold surface exposed the disk shaped ends of the Au nanowires which is the active electrode area. From cyclic voltammetry experiments, the detection limit of the NEE is three orders of magnitude lower than that

at a conventional gold disk electrode with equivalent geometric area.[42] These results between the double-layer charging current are three orders lower at the NEE. Cyclic voltammetry is generally considered to be a poor electroanalytical technique. This is because the high double-layer charging currents observed at a macroelectrode make the signal-to-background ratio low. The electrochemical response at the NEE demonstrates that cyclic voltammetry can be a very powerful electroanalytical technique.[83]

In addition to the above applications, these Au nanotube membranes can mimic the function of a ligand gated ion channel.[84] They can be switched from an "off" state to an "on" state in response to the presence of a chemical stimulus. The off state was obtained by making the membrane hydrophobic, and the on state was obtained by introducing ions and electrolytes into the membranes. The pores with ~ 2 nm diameter were rendered hydrophobic by chemisorbing octadecylthiol. It was shown that a long chain ionic surfactant (1-dodecanesulfonic acid) would partition into the hydrophobic membrane causing the pores to flood with water, showing that the membrane supported an ion current and the off state was transitioned to the on state.[84]

These membranes can also be used as sensors for the determination of ultratrace concentration of ions and molecules.[74,75,85] In this case, two salt solutions were separated by the nanotube membrane, a constant transmembrane potential was applied, and the resulting transmembrane current was measured. When an analyte of comparable dimensions to the inside diameter of the nanotubes was added to one side of the membrane, a decrease in transmembrane current was observed. The magnitude of this drop in transmembrane current was proportional to the analyte concentration. Detection limits as low as 10^{-11} M were obtained.[75]

Finally the nanowires have been shown to be useful as building blocks for self-assembly of supramolecular architectures. The nanowire membranes were immersed in a dithiol solution, and then the membrane was immersed into an aqueous suspension of the colloidal Au nanoparticles. In this way, a Au nanowire/Au colloidal assembly can be obtained.[86]

We have seen that the inside diameters of the Au nanotubes are monodisperse, the pore size of the membranes can be easily controlled over a very large range and the membrane surfaces are easy to be modified because of the well-known gold-thiol chemistry. This leads us to ask, "Could these membranes be used to separate proteins on the basis of size, shape, charge, or chemical properties?" Chapter 2 will give thorough details of protein separation investigation with engineered gold nanotube membranes. An overview of protein separation via membrane ultrafiltration techniques will first be discussed below.

Protein Separations with Membrane Ultrafiltration Techniques

The rapid growth in the fields of biotechnology, food processing, and biomedical applications has led to an increased demand for efficient and large-scale protein separation processes.[87-89] Currently, the most commonly used protein separation techniques are chromatographic techniques. These techniques have high selectivity to separate proteins. However, large-scale separations are expensive and time-consuming since these techniques require relatively more complex instrumentation to run efficiently while resulting in low product yields. Hence, a separation technique that can yield high throughput of product at low process cost would be welcomed by the biotech industry.

Compared to other methods, membrane ultrafiltration techniques offer the potential advantages of lower cost, higher speed, and ease of transition to large-scale

commercial production. There has been considerable interest in this type of protein separation.[87-91] Polymeric materials used to prepare ultrafiltration membranes include polycarbonate, polyvinylidene fluoride, polysulphone, polyethersulphone, cellulose acetate and regenerated cellulose.[87-91] In some cases, the morphology of the membrane are sophisticated. For example, polysulfonic membrane has a dense thin skin side that is supported by a more porous open structure, this morphology allows for high selectivity without sacrificing flux. These membranes have either straight-pore structure, or fibrous structure, or nonsymmetrical porous structure. In ultrafiltration membrane techniques, fibrous and nonsymmetrical membranes are commonly used because of high porosity (up to 80%). These commercially available membranes come in limited pore sizes.

Ultrafiltration is not purely a size based separation process, and other interactions can significantly affect its performance. These include the interactions between solute and membrane as well as between solute and solute. For a given membrane, selectivity can be improved by increasing flow hydrodynamics, adjusting solution physiochemical conditions such as pH and salt concentration, and pre-treatment of the membrane surface.[87-90]

It is important to select the best pH and ionic strength of the protein solution, which can adjust the interactions between solute and membranes as well as between solute and solute.[88, 92, 93] Since different proteins have different isoelectric points (pIs), proteins have different charges at different pH. The charges on a protein molecule result in an electrical double layer surrounding the proteins, which will change the effective volume of the protein molecule in the solution. For this reason ionic strength affects the effective volume of a protein molecule. Therefore adjusting pH and salt concentration can

promote the charge effect and change the effective volume of proteins to achieve effective separation of two proteins. The ultrafiltration processes normally operate with constant transmembrane pressure.[87] Transmembrane pressure can reduce membrane fouling and increase throughput.[87] It is well known that increasing the transmembrane pressure results in increasing permeate flux until a threshold pressure is reached.[87]

Membrane ultrafiltration techniques are compromised however by limitations of the process filtration. These limitations include broad pore size distribution of the membranes, concentration polarization, membrane fouling, solute-solute interactions, and solute-membrane interactions.

High resolution separation in ultrafiltration can be obtained by careful selection of device operating conditions such as module design and process configurations, and physiochemical solution properties especially pH and ionic strength of the solution. These appropriate conditions will decrease the limitations for ultrafiltration and adjust the interactions between solute and solute as well as between solute and membrane.

Plasma Based Etching

Plasma etching, a dry etching process, has become a very useful means of removing small quantities of material from a variety of substrates quickly and efficiently.[94] Plasma processes have been used in many highly sensitive integrated applications to precisely remove specific materials from sample surfaces. To generate plasma, a pair of electrodes is needed, one is connected to a radio frequency (RF) voltage and the other one is grounded. RF energy is applied to the electrodes which accelerates electrons to increase their kinetic energy. The electrons collide with a neutral gas to form a collection of gaseous species including ions, free radicals, electrons, photons and neutrals.[94] The gaseous species can react with the surface to be etched such that reaction

product is volatile and can be pumped away. There are several types of etching--physical etching (anisotropic), chemical etching (isotropic) and reactive ion etching (combination of physical etching and chemical etching). Usually in plasma based etching, both chemical etching and physical etching occur.[94]

There are many applications for plasma etching such as photoresist removal, glass-like compound etching (e.g., SiO_2) and polymer etching to produce microstructures and nanostructures. For example, large-area, well-ordered, periodic nanopillar arrays with lateral dimensions as small as 40 nm have been developed based on a combination of colloidal lithography and plasma etching techniques.[95,96] The etching masks on silicon substrates were prepared using the close-packed structures formed by monodisperse polystyrene beads.[95,96] Polymer surfaces can also be modified by a plasma treatment, for example, to improve wetting properties and to enhance the adhesion of plasma-deposited coatings.[97]

In this research, a plasma etching technique was used to generate nanostructures. In Chapter 3, oxygen plasma etching was used to expose the nanowires from a template membrane. In Chapter 4, nanowells were generated by argon plasma etching using nanoporous alumina membranes as masks.

Dissertation Overview

The goals of this research have been to develop nanostructures using nanofabrication and nanopatterning methods and to investigate potential applications of these nanostructures in chemical separations and sensors. The previous part of Chapter 1 has reviewed background information for this dissertation including membrane-based template synthesis, applications of gold nanotube and nanowire membranes synthesized

by electroless gold plating of template synthesis, protein separation with membrane ultrafiltration technique, and plasma based etching technique.

In Chapter 2, template-based synthesis was used to prepare gold nanotube membranes. The membranes were easily modified with poly(ethylene glycol) to prevent protein adsorption. The application of these engineered gold nanotube membranes to protein separations has been investigated. The membranes have narrow pore size distribution and controllable pore size; therefore they have high protein transport selectivity. Because of the low transport rate resulting from nanopore size, two types of driving forces were applied to increase transport flux-transmembrane pressure and transmembrane potential. The effect of pore size, protein charge and solution pH on protein transport selectivity have been investigated. In addition, gold nanotube membranes are ideal model systems for exploring the flux-vs.-selectivity tradeoff in membrane-based protein separations due to the controllable pore sizes.

Chapter 3 deals with the issue of using template-synthesized nanowires as building blocks for preparing supramolecular architecture. In an approach (developed previously in this lab) assembly was achieved by reacting the ends of the nanowires embedded in a template membrane with colloidal gold particles. The efficiency of assembly was low because the nanowire ends were often recessed in the membrane. This chapter describes the method developed to increase the efficiency of nanowires as building blocks. I have used oxygen plasma etching to remove part of the polymer template and leave the nanowire ends exposed. By adjusting the etching time, the length of the protruding nanowires can be controlled. In addition to possible applications in

self-assembly, these protruding nanowires could possibly be used to increase electrical contact between the nanowire containing membrane and a substrate metal surface.

In Chapter 4, highly ordered alumina membranes were used as masks to etch substrates such as glass to obtain arrays of nanowells in the glass surface. The depth of the nanowells can be controlled by varying the etch time. Field emission scanning electron microscopy (FESEM) and atomic force microscopy (AFM) were used to characterize the nanopatterns and obtain the depth of the etched nanowells. I have shown that the portions of the glass surface inside vs. outside of the nanowells can be functionalized with different chemical species. Friction measurements from the atomic force microscope were used to demonstrate this differential functionalization. In addition, after the nanowells were modified with molecular linkers, nanoparticles modified with complementary corresponding molecular linkers were selectively attached to the specific location. The results and conclusions of the work presented in this dissertation are summarized in Chapter 5

CHAPTER 2
PROTEIN TRANSPORT IN ENGINEERED GOLD NANOTUBE MEMBRANES

Introduction

There is increasing interest in using synthetic membranes for protein separations.[98-101] Potential advantages of membrane-based protein separations include low cost, high speed, and high throughput. In addition, membrane-based separations can, in principle, be easily scaled up for use in large-scale commercial production.[99] Synthetic membrane materials investigated to date for protein separations include polysulfone,[98, 99, 101] polycarbonate,[102, 103] polyvinylidene fluoride,[104] polyethersulfone[105, 106] and regenerated cellulose.[98, 107, 108] A number of problems must be overcome before membranes can be more widely utilized for industrial protein separations. These include the broad pore-size distribution obtained with most synthetic membranes, which compromises selectivity, and membrane fouling caused by adsorption of proteins onto the surfaces or within the pores of membrane.[109-113]

We, and others, have been exploring the transport properties of gold nanotube membranes[44, 71-73, 78, 114, 115] prepared via the template method,[4-6] a general approach for making nanomaterials. The gold nanotubes are prepared by electrolessly plating Au within the pores of a track-etched polycarbonate filter. These templates have cylindrical pores with monodisperse diameters that run through the entire thickness of the membrane. The outside diameter of the gold nanotubes obtained is determined by the pore diameter of the template, and the inside diameter is determined by the electroless deposition time. The inside diameter can be controlled at will from tens of nanometers

down to less than one nanometer.[72, 73, 116, 117] As a result, these membranes can be used in a simple membrane-permeation experiment to cleanly separate small molecules on the basis of molecular size.[72] In addition, ion transport selectivity can be introduced by electrostatically charging the membrane to put either excess positive charge or excess negative charge on the Au nanotubes.[44, 114] Ion and chemical transport selectivity can also be introduced by chemisorbing thiols to the Au nanotube walls.[71, 73, 79, 115] By appropriate choice of thiol, membranes that preferentially transport cations or anions and hydrophobic or hydrophilic molecules can be prepared. This ability to independently and precisely control both the inside diameter and chemical characteristics of the nanotubes make these membranes ideal model systems for studying how pore size, chemistry and charge affect rate and selectivity of permeate transport in membranes.

Protein transport has recently been investigated in the Au nanotube membranes.[116-118] In this case, the ability to tailor the chemistry of the nanotubes provides a route for suppressing protein adsorption and thus fouling, a vexing problem for ultrafiltration separations of proteins.[104, 113, 119-122] In particular, there have been a number of investigations of protein transport in the track-etched polycarbonate membranes[100, 103, 109, 111, 112, 123] used as the templates to prepare the Au nanotubes, and protein adsorption has proven to be a problem in such studies.[109, 111, 112, 123] It is well known that PEG-modified surfaces show decreased protein adsorption relative to the unmodified surface.[124-129] With the Au nanotube membranes, membrane chemistry can be controlled by chemisorbing thiols to the surface of the membrane and the walls of the Au nanotubes.[71, 73, 79, 115] Of particular relevance to the work described here, protein adsorption to the Au nanotube membranes was suppressed by chemisorbing a thiol-terminated poly(ethylene

glycol) [117] The ability to precisely control the inside diameter (ID) of the nanotubes (and to produce nanotubes with very monodisperse IDs) is also advantageous in that this should allow for size-based separation of proteins of similar molecular weights. This can be a problem for conventional ultrafiltration membranes, which typically have a broad distribution of pore sizes. Because the inside diameters of the nanotubes can be controlled at will, these membranes are ideal model systems for exploring how pore size affects rate and selectivity of protein transport. Such studies are important because it is almost always the case in membrane-based separation systems that membranes with high fluxes show lower selectivities and membranes with low fluxes show higher selectivities.[71-73]

This work includes the investigations of protein separations in the gold nanotube membranes using two types of driving force–transmembrane pressure and transmembrane potential–to increase protein flux through the membranes. Transmembrane pressure was applied to the feed solution side to force the solution through the membrane. In this case, the effect of nanotube inside diameter on rate and selectivity of protein transport was investigated for three proteins–lysozyme (Lys), bovine serum albumin (BSA) and β-lactoglobulin A. Electrophoretic transport is accomplished by applying a potential difference across the membrane. The transport properties of four proteins of differing sizes and pI values–lysozyme, bovine serum albumin, carbonic anhydrase, and bovine hemoglobulin–were investigated. In this work, the effects of nanotube inside diameter, solution pH, and applied transmembrane potential on the rate and selectivity of protein transport in the PEG-thiol treated gold nanotube membranes were investigated.

Experimental

Materials

Polycarbonate template membranes (6 μm thick) with 30 nm, 50 nm or 100 nm diameter pores were obtained from Poretics. The pore densities were 6×10^8 pores/cm^2 (30 nm, 50 nm) and 4×10^8 pores/cm^2 (100 nm). A commercial gold-plating solution (Oromerse SO Part B, Technic Inc.) was used to deposit the Au nanotubes within the pores of these membranes.[73] Anhydrous $SnCl_2$, $AgNO_3$, trifluoroacetic acid, Na_2SO_3, NH_4OH, formaldehyde, anhydrous methanol, and sodium phosphate (monobasic and dibasic) were used as received. The proteins lysozyme (Lys, pI = 11, MW = 14 kDa), β-lactoglobulin A (LGA, MW = 36 kDa), bovine serum albumin (BSA, pI = 4.9, MW = 67 kDa), bovine hemoglobin (Hb, pI = 7.0, MW = 65 kDa) and carbonic anhydrase (CA, pI = 6.2, MW = 29 kDa) were purchased from Sigma-Aldrich and used as received. Thiol-terminated poly(ethylene glycol) (PEG-thiol, MW = 5000 Da) was obtained from Nektar Therapeutics (previously as Shearwater Polymers). Purified water was prepared by passing house-distilled water through a Millipore Milli-Q water purification system. Regenerated cellulose membranes (molecular weight cutoff (MWCO) = 3500 Da) were obtained from Spectrum Laboratories, Inc. Prior to use, these membranes were rinsed with water for at least 30 minutes to remove glycerine which acted as a humectant.

Membrane Preparation

The plating method used to deposit the Au nanotubes within the pores of the template membranes has been described previously.[73] With this method, Au is deposited on the walls of the pores yielding Au nanotubes that span the complete thickness of the membrane. The inside diameter of these nanotubes can be controlled at will by varying

the plating time.[73] In addition to the nanotubes lining the pore walls, each face of the membrane is coated with a thin gold surface film. These films however do not block the mouths of the nanotubes at the membrane surfaces.

Membranes having Au nanotubes with inside diameters (IDs) in the range of 20 nm to 60 nm were used for these studies. Membranes containing Au nanotubes with IDs less than 30 nm were prepared in the templates with 30 nm-diameter pores. Membranes containing nanotubes with IDs in the range 30 nm < ID < 50 nm were prepared in the templates with 50 nm-diameter pores. Membranes containing Au nanotubes with IDs greater than 50 nm were prepared in templates with 100 nm-diameter pores. A gas-flux method described previously[73] was used to obtain the IDs of the Au nanotubes. The ID values reported here were measured before chemisorption of the PEG-thiol. The PEG-thiol was chemisorbed to the Au by immersion of the nanotube membrane for 6 days into a degassed 1 mM solution of this thiol, which yields a PEG layer along the nanotube walls. XPS measurements on a similar 5000 MW PEG-thiol on Au surface showed that the thiol layer thickness is ~2.4 nm.[124] The thiolated PEG was chemisorbed to the nanotube walls and Au surface films to prevent protein adsorption on the membrane.[117]

Protein Transport Experiments

Applied transmembrane pressure

The Au nanotube membranes were mounted between the two halves of a U-tube permeation cell as described previously.[73] Figure 2-1 shows the schematic of transport cell when applying transmembrane pressure. Both single-protein and two-protein permeation experiments were done. The single-protein experiments were done on Lys and BSA, while the two-protein experiments were done on BSA/Lys and BSA/LGA. In the single-protein experiments, the feed half-cell contained 5 mL of 20 mM sodium

phosphate buffer solution (pH = 7 0) that was 0 050 mM in the desired protein. Unless otherwise noted, this solution was forced through the membrane by applying 20 psi pressure to the feed half-cell. The permeate half-cell was initially empty. As solution

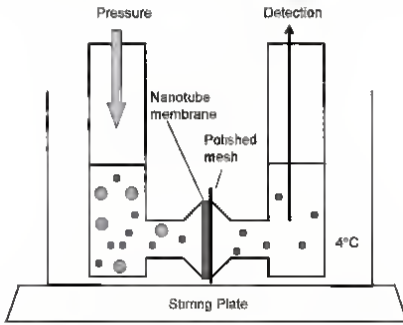

Figure 2-1 Schematic of the transport cell with applied pressure The applied pressure is 20 psi.

was forced through the membrane, the permeate half cell was periodically sampled and the concentration of the protein was determined via the UV absorbance at 280 nm using a Hitachi U-3502 spectrophotometer The two-protein permeation experiments were done in an analogous fashion except the feed solution was 0 025 mM in each protein. The concentration of each protein in the permeate half-cell was determined by sampling the permeate solution after ~1 mL was transported and doing HPLC analysis. A Shimadzu HPLC system with an YMC-Pack aqueous SEC (diol phase) column and UV/Vis detector (280 nm) was used. The mobile phase was 0 1 M phosphate buffer (pH = 6.8) containing 0 2 M NaCl, the flow rate was 1 0 mL/min. In addition to these pressure-driven transport

experiments, preliminary single-molecule permeation experiments were done in the absence of applied pressure. In this case, transport occurred by diffusion of the protein across the membrane into 5 mL of the buffer solution.

Applied transmembrane potential

A four-compartment cell (Figure 2-2) was employed to study the effect of applied transmembrane potential. The outer compartments contain electrolyte that is devoid of protein and are in contact through regenerated cellulose membranes with both the feed-cell and the permeate-cell compartments. A Pt wire electrode (length 15.2 cm, diameter = 0.81 mm) was inserted into each outer electrolyte solution, and these electrodes were used to apply a constant potential across the membrane. When the applied potential was ≤10 V, a potentiostat (MSTAT4+, Arbin Instruments) was used, for potentials >10 V, a high voltage power supply (FB1000, Fisher Scientific) was used. The following sign convention was employed: For positive applied potentials, the anode was in the compartment adjacent to the feed solution and the cathode was in the compartment adjacent to the permeate solution. The polarity was reversed for negative applied potentials. The volume of each compartment was ~ 6 mL, and 4 mL of solution were added to each compartment.

The rate of protein transport across the membrane was determined by periodically assaying the permeate solution for the protein. Experiments in which the feed solution contained only one protein and in which the feed solution contained two proteins were conducted. The single-protein transport experiments were done on Lys and BSA. Two-protein transport experiments were done on Lys/BSA, Hb/CA and Hb/BSA. Unless otherwise noted, the concentration of protein in the feed solution for the single-protein experiments was 0.050 mM. For the two-protein experiments the feed solution was 0.025

mM in each protein. In addition to experiments with a constant applied transmembrane potential, in some experiments the protein molecules were simply allowed to diffuse down their concentration gradients across the membrane and into the permeate solution.

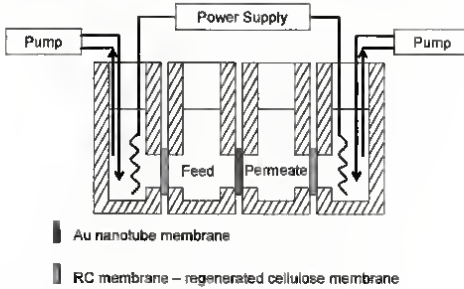

Figure 2-2. Schematic of the four-compartment transport cell.

The electrolyte in all four of the compartments in Figure 2-2 was a phosphate buffer solution (40 mM ionic strength), the pH was adjusted to the desired value by varying the ratio of the dibasic and monobasic salts used. The electrophoretic current is supported at the electrodes in the outer compartments by oxidation and reduction of water, and this produces H^+ in the anode compartment and OH^- in the cathode compartment. To insure that this did not cause a change in pH, fresh buffer solution was continuously pumped through the outer compartments. A Watson-Marlow Pump Pro MPL Multichannel Cartridge Pump with 1.14 mm diameter tubing was used. Two channels of the pump delivered fresh buffer from a reservoir to the bottoms of the outer compartment cells, and another two channels withdrew an equivalent amount of "used"

buffer from the top of the cells and sent it to waste. Both the feed and permeate compartments were magnetically stirred during the permeation experiments. Because our previous studies showed that lower temperatures prevented protein aggregation,[117] all transport experiments were done at 4 °C.

In the single-protein transport experiments, the concentration of protein in the permeate solution was determined by UV absorbance using a Hitachi U-3502 spectrophotometer. The wavelengths used for these analyses were 280 nm for Lys, CA and BSA and 405 nm for Hb. For the Lys/BSA two-protein transport experiments, the concentrations of these proteins in the permeate solution was determined using an HPLC method. The HPLC method was required because the UV absorption spectra for Lys and BSA overlap. However, Hb absorbs strongly at 405 nm, where the other proteins do not absorb. For this reason, HPLC was not required to determine protein concentrations in the permeate for the Hb/CA and Hb/BSA two-protein transport experiments. Instead, the concentration of Hb was determined from the absorbance at 405 nm, and the absorbance at 280 nm was corrected for this amount of Hb to provide the concentration of the second protein.

Results and Discussion

Figure 2-3 shows results of single-protein (Lys) permeation experiments in the absence of applied pressure for ID = 23-nm Au nanotube membranes, with and without chemisorbed PEG-thiol. Without the PEG-thiol, transport stops after ~ 8 hours, indicating rapid blockage of the nanotubes by adsorbed protein. In contrast, when the PEG-thiol is present, linear moles-transported vs. time data are obtained for up to five days. These data clearly show that protein adsorption is prevented, or is very strongly suppressed, by the chemisorbed PEG. This suppression of protein adsorption is also

observed in the pressure-driven transport experiment, where protein flux is ~ 2-orders of magnitude higher Indeed, we have conducted such experiments for as long as six days with no evidence for protein adsorption.

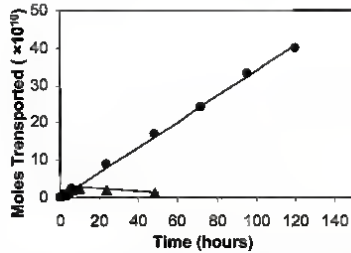

Figure 2-3 Plots of moles transported vs time for Lys diffusion (no applied pressure) across ID = 23-nm Au nanotube membranes. Upper line–with chemisorbed PEG-thiol. Lower curve–no PEG thiol

Applied Transmembrane Pressure

All data presented in this section are from membranes with chemisorbed PEG-thiol and where 20 psi pressure was used to drive the feed solution through the membrane

Figure 2-4 shows results of single-protein permeation experiments for Lys (upper line) and BSA (lower line) through a membrane with ID = 40 nm nanotubes. The flux of Lys is 4-times higher than the flux of BSA. The Stokes radii for BSA and Lys are 3 6 nm and 2 nm, respectively.[130] hence, the Stokes-Einstein equation would predict that in free solution the diffusion coefficient for Lys would be only 1 8 times higher than that for BSA. That the ratio of the fluxes in the nanotube membrane (Figure 2-4) is higher than

this Stokes ratio is indicative of hindered transport[78, 131] of the protein molecules in these nanoscopic tubes. Two-protein permeation experiments were used to explore this issue further.

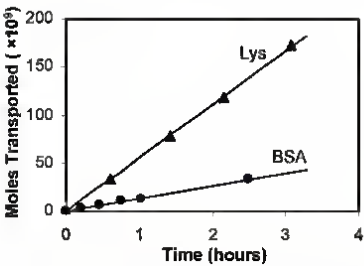

Figure 2-4. Plots of moles transported vs. time for Lys (upper) and BSA (lower) across an ID = 40-nm Au nanotube membrane. Single-protein permeation experiments.

Figure 2-5A shows HPLC data for the feed solution from a BSA/Lys two-protein permeation experiment. Figure 2-5B shows HPLC data for an aliquot of the permeate solution after permeation through an ID = 45 nm nanotube membrane. In analogy to the single-protein transport case (Figure 2-4), the attenuation of the BSA peak, relative to the Lys peak, clearly shows the enhanced discrimination against the larger protein molecule. Figure 2-5C shows analogous data after transport though an ID = 30-nm nanotube membrane; now the BSA peak is barely discernable. BSA could not be detected in the permeate from an ID = 20-nm nanotube membrane (Figure 2-5D). This, of course, does not mean that there is no BSA present; it simply means that the concentration is below the detection limit of our analytical method, which for BSA is ~0.2 μM. In an attempt to

obtain a discernable BSA signal in the permeate from the ID = 20-nm nanotube membrane, we increased the permeation volume from 1 to 2 mL, but there was still no detectable BSA in the permeate

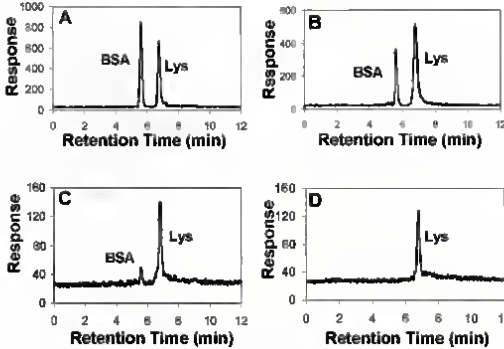

Figure 2-5 HPLC data for two-protein (Lys/BSA) permeation experiments (A) Feed solution. Permeate solutions after transport through ID = 45-nm (B), 30-nm (C), and 20-nm (D) nanotube membranes.

The transport data in Figure 2-5 can be quantified by defining a Lys vs. BSA selective coefficient, $\alpha_{Lys/BSA}$, which is the ratio of the concentration of Lys to the concentration of BSA in the permeate solution. Table 2-1 shows that $\alpha_{Lys/BSA}$ increases with decreasing nanotubule diameter. Analogous results were obtained for small-molecule permeation in smaller-ID Au nanotube membranes [72, 78] and was explained in terms of hindered transport,[78, 131] which occurs when the diameter of the molecule approaches the diameter of the pore in which it is being transported. This issue was

discussed in some detail in a prior publication from our group.[78] In the case of the ID ~ 20-nm membrane, where BSA could not be detected, a minimal transport selectivity coefficient is reported, defined as before[72] as the detected concentration of the smaller protein (Lys) divided by the detection limit for the larger protein (BSA). As indicated in Table 2-1, the selectivity coefficient for the ID = 20-nm nanotube membrane is at least 20. Table 2-1 also shows that the increased selectivity for the membranes containing the smaller ID nanotubes comes at a price—the concentration of both proteins in the permeate decreases with decreasing nanotube diameter. Hence, as is typically observed in membrane-based separations processes, membranes that show higher selectivity also show decreased permeate throughput or productivity.[132]

Table 2-1. Concentration of proteins in the permeate and transport selectivity coefficients for two-protein (Lys/BSA) permeation experiments

ID (nm)	Conc. of Lys (μM)	Conc. of BSA (μM)	$\alpha_{Lys/BSA}$
20	4.0	Detection limit	≥20
30	6 3	0.5	13
45	18 8	8 4	2.2

Table 2-2. Concentration of proteins in the permeate and transport selectivity coefficients for two-protein (LGA/BSA) permeation experiments

ID (nm)	Conc. of LGA (μM)	Conc. of BSA (μM)	$\alpha_{LGA/BSA}$
22	3 1	Detection limit	>15
27	4 3	0 3	14
40	10 5	1.6	6 7

Figure 2-6 shows analogous data for the separation of BSA from LGA and the corresponding selectivity coefficients are also tabulated in Table 2-2. Again, we see

higher selectivity and lower productivity for the membranes containing the smaller ID nanotubes.

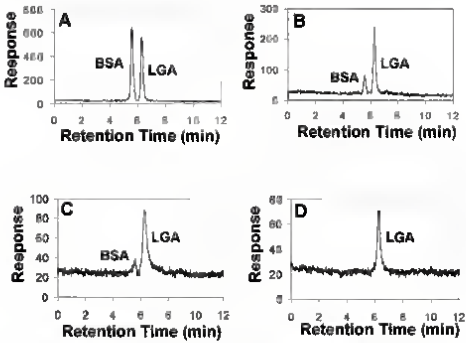

Figure 2-6 HPLC data for two protein (LGA/BSA) permeation experiments. (A) Feed solution. Permeate solutions after transport through ID = 40-nm (B), 27-nm (C), and 22-nm (D) nanotube membranes.

Applied Transmembrane Potential

Single-protein transport experiments

At pH = 7 Lys is positively charged, and a positive applied cell potential should result in electrophoretic transport of Lys from feed to permeate. This is illustrated by the data in Figure 2-7, which show the effect of applied potential on the Lys flux in a membrane with 40 nm ID Au nanotubes. When +6 V was applied (time, $t < 2$ h and again at 4 h $\leq t \leq$ 6 h), the flux is substantially higher than when no potential is applied (2 h $< t <$ 4 h). In contrast, when –6 V was applied ($t >$ 6 h), the direction of Lys

electrophoresis was from permeate to feed, and the concentration of Lys in the permeate decreased during this time interval. Thus shows that at this negative applied potential, the diffusive flux of Lys from feed to permeate is overwhelmed by the electrophoretic flux from permeate to feed.

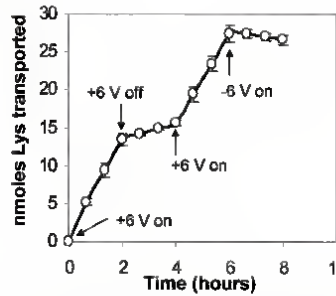

Figure 2-7 Plot of nmoles of Lys transported vs time in a membrane with 40 nm ID nanotubes with and without an applied transmembrane potential of +6 V

The effect of the magnitude of the applied potential on the Lys flux (J_{Lys}) can be quantified by considering the diffusive and electrophoretic terms of the Nernst-Planck equation.[1]

$$J_{Lys} = - D_{Lys}(dC_{Lys}/dx) - (a_{Lys}F/RT)\, D_{Lys}C_{Lys}(d\Phi/dx) \qquad (1)$$

D_{Lys}, C_{Lys}, and a_{Lys} are the diffusion coefficient, concentration and effective charge of Lys and dC_{Lys}/dx and $d\Phi/dx$ are the concentration and electric field gradients across the membrane. The first term in Equation 1 describes diffusive transport, and the second is the electrophoretic transport term. In principle, there could also be an electroosmotic

transport term,[133] but because an electrical neutral thiol was chemisorbed to the nanotube walls, this term is negligible. According to Equation 1, a plot of flux vs. applied transmembrane potential should be linear, and Figure 2-8 (upper curve) shows that this is, indeed, the case. Hence, applying a transmembrane potential provides a route for enhancing flux or throughput in a membrane-based protein separation process.[102, 103, 134]

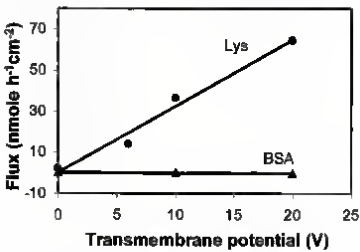

Figure 2-8. Plots of flux vs. applied transmembrane potential for Lys and BSA. Membrane as per Figure 2-7.

In contrast to Lys, BSA is negatively charged at pH = 7, and as a result, Lys and BSA move in opposite directions in an electric field. This is illustrated by the lower curve in Figure 2-8, which shows results of analogous single-protein permeation experiments for BSA at positive applied transmembrane potentials. The BSA flux decreased from 0.4 nmole h^{-1} cm^{-2} (no applied potential) to 0.07 and –0.31 nmole h^{-1} cm^{-2} for transmembrane potentials of +10 and +20 V, respectively. The negative flux at +20 V indicates that the net direction of transport of negatively charged BSA is now from

permeate to feed. This shows, again, that the diffusive flux from feed to permeate is now overwhelmed by the electrophoretic flux from permeate to feed.

As will be discussed in greater detail below, these data show that when two proteins are oppositely charged, electrophoresis can be used to improve membrane-transport selectivity. However, there is also a molecular-sieving contribution to the transport selectivity. This is illustrated earlier in Figure 2-4 by comparing the Lys and BSA fluxes with no applied transmembrane potential (diffusive fluxes), which indicates that hindered diffusion[131] of these protein molecules occurs in these nanoscopic tubes. This has also been observed for other molecules in these membranes, and this concept is discussed in greater detail in a recent review [78]

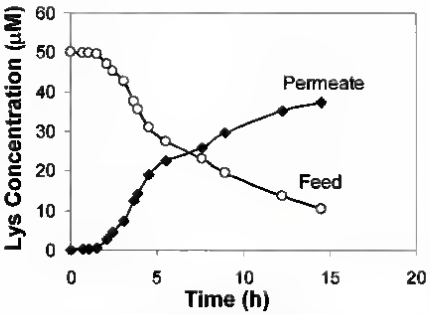

Figure 2-9. Lys concentration vs. time in the permeate and feed solutions during a permeation experiment. The following transmembrane potentials used: 0 V for $t \leq 1.5$ h, +10 V for $1.5\text{ h} < t \leq 3$ h, +20 V for $t > 3$ h. Membrane as per Figure 2-7.

Finally, Figure 2-9 shows plots of the concentrations of Lys in the feed and permeate solutions vs. time during a transport experiment using various values of applied transmembrane potential. After 6-8 hours, the concentration of Lys in the permeate is greater than that in the feed, and Lys is being driven electrophoretically up its concentration gradient. This would, of course, not be possible in an experiment where diffusion is the only mode of transport. This ability to drive, in principle, all of a desired protein out of the feed solution is an important advantage of the electrophoretic transport experiment.

Lys/BSA two-protein transport experiments

As noted above, the ability to control nanotube ID makes these membranes ideally suited for fundamental investigations of the selectivity-vs.-flux tradeoff observed in membrane-based separations.[71-73] The separation of Lys from BSA is first conducted at pH = 7, in membranes containing nanotubes with IDs of 20-40 and 60 nm, and with an applied transmembrane potential of +8 V. The concentration of Lys in the permeate solution was periodically monitored, and permeation experiments were continued until 60% of the Lys was transported to the permeate solution. At this point, the concentration of BSA in the permeate was also determined, and the Lys/BSA selectivity coefficient was calculated as follows, where the subscript p indicates concentrations in the permeate solution:

$$\alpha_{Lys/BSA} = [Lys]_p / [BSA]_p \qquad (2)$$

For these experiments, the flux is an average value obtained by dividing the total number of moles Lys transported by the time required to transport 60% of the Lys to the permeate solution, and by the membrane area. As would be expected, the Lys flux

increases with nanotube ID (Figure 2-10) This increase in flux comes at a price, in that the selectivity coefficient decreases with increasing nanotube ID Hence, we see the tradeoff between flux and selectivity typically observed for membrane-based separation processes [71 73] However, even for the largest ID nanotube, the selectivity is quite good, $\alpha_{Lys/BSA} = 22$ For the smallest ID nanotube, BSA could not be detected in the permeate. In this case the selectivity coefficient is a minimal value defined, as before,[117] as the measured concentration of Lys in the permeate solution divided by the detection limit of the HPLC-based BSA analysis (0.2 μM) The value of this minimal selectivity coefficient, $\alpha_{Lys/BSA} > 75$, indicates that excellent selectivity can be obtained. It is important to emphasize again that there are two factors contributing to this excellent selectivity–the small nanotube size, which discriminates against the larger BSA molecule, and the difference in charge between the proteins to be separated.

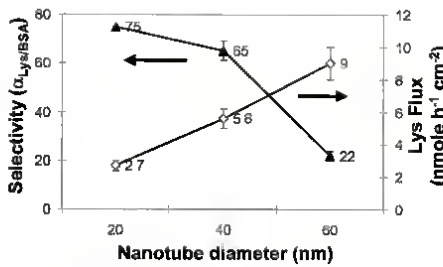

Figure 2-10 Selectivity and flux vs nanotube ID for the Lys/BSA separation. pH = 7 Transmembrane potential = +8 V

It is of interest to compare the Lys fluxes obtained for this two-protein transport experiment with analogous Lys flux values obtained from single-protein transport experiments. For each nanotube ID, the flux of Lys in the single-protein experiment is twice as high as in the two-protein experiment (Table 2-3). These data indicate that the presence of BSA in the nanotubes in the two-protein experiment hinders the transport of Lys. The factor of 2 for each nanotube ID is, however, fortuitous. This is because for the 20 nm ID nanotubes, the very low amount of BSA transported (highest $\alpha_{Lys/BSA}$ value, Figure 2-10) indicates that there is a very small amount of BSA present in the nanotube at any time. However, the small nanotube ID also means that it is easier for any BSA that is present to hinder the Lys transport. For the 60 nm ID nanotubes there is clearly more BSA present in the nanotube at any time (lowest $\alpha_{Lys/BSA}$ value, Figure 2-10), but the large nanotube ID means that it is easier for the Lys molecules to evade the BSA molecules.

Table 2-3 Comparison of average Lys flux values obtained from two-protein (Lys/BSA) and single-protein (Lys) transport experiments.

Nanotube diameter (nm)	Two-protein flux (nmole hr^{-1} cm^{-2})	Single-protein flux (nmole hr^{-1} cm^{-2})
20	2.7 ± 0.3	6.3 ± 0.5
40	5.6 ± 0.6	12 ± 1
60	9 ± 1	20 ± 2

Figure 2-10 shows that for the 20 nm ID nanotubes a transmembrane potential of +8 V is sufficient to essentially shut down BSA transport. This +8 V potential did not, however, completely shut down BSA transport in the membranes with the larger ID nanotubes, and as a result lower Lys/BSA selectivity coefficients were obtained (Figure 2-10). The question then becomes–what potential is sufficient to essentially shut down BSA transport in the membranes with the two larger ID nanotubes?

To explore this issue we conducted Lys/BSA transport experiments as a function of applied potential for each nanotube ID. Each experiment was continued until 80% of the Lys initially present in the feed was transported to the permeate (i.e., final concentration of Lys in the permeate = 20 μM). For each nanotube ID we determined the minimum voltage needed to make BSA undetectable in this permeate solution. Since the detection limit for BSA is 0.2 μM this means that we are finding the voltage required for each nanotube ID to yield an $\alpha_{Lys/BSA}$ value of at least 100.

Table 2-4. Transmembrane potential required to shut down BSA transport in membranes having nanotubes with the indicated diameters. Two-protein Lys/BSA transport experiments. The corresponding average Lys flux values and the time required to obtain a Lys/BSA selectivity coefficient of ≥100 are also shown.

Nanotube diameter (nm)	Transmembrane potential (V)	Lys flux (nmole h^{-1} cm^{-2})	Time (h)
20	5	2.5 ± 0.3	65
40	20	8.5 ± 0.5	25
60	35	29 ± 3	5.7

As would be expected, the voltage required to shut down BSA transport increases with nanotube ID (Table 2-4). There is however, a clear advantage of using membranes with larger ID nanotubes operating at higher transmembrane voltages–the flux of Lys is maximized, and the time required to affect the separation is minimized (Table 2-4). Put another way, this strategy of applying higher potentials across membranes with larger ID nanotubes provides a way to beat the selectivity-vs-flux tradeoff. This is, because with all of the nanotubes in Table 2-4 we have obtained the same excellent selectivity, $\alpha_{Lys/BSA}$ =100, but with the combination of 60 nm ID nanotubes and +35 V we maximize the flux as well. The caveat is that this advantage obtained by using higher transmembrane

voltages with membranes that have larger ID nanotubes will only be observed when the proteins have opposite charges where molecular-sieving selectivity is not required When the proteins to be separated have the same charge, molecular sieving is required to accomplish the separation, and high selectivity can only be obtained with membranes containing small ID nanotubes (see below)

CA/Hb two-protein transport experiments

At pH = 4 5 both CA and Hb are positively charged. However, because Hb has a higher pI the magnitude of the positive charge on the Hb molecule is greater than that of the CA molecule Hence, in the absence of molecular sieving effects, the electrophoretic flux of Hb should be greater than that of CA at pH = 4 5. That the experimentally observed flux of CA is always higher than that of Hb ($\alpha_{CA/Hb} > 1$, Figure 2-11) shows that the selectivity in this case is dominated by the molecular-sieving effect in that Hb (65 kDa) is substantially larger than CA (29 kDa).

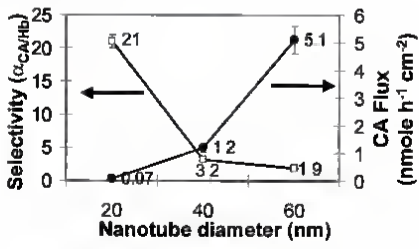

Figure 2-11 Selectivity and flux vs nanotube ID for the CA/Hb separation. pH = 4 5 Transmembrane potential = +8 V

Figure 2-11 shows the flux/selectivity tradeoff for the CA/Hb pair when a transmembrane potential of +8 V was applied. In analogy to Figure 2-10, the average CA flux increases, and $\alpha_{CA/Hb}$ decreases, with increasing nanotube ID. For any value of nanotube ID, the selectivity coefficient for the CA/Hb case is substantially smaller than for the Lys/BSA case. This is a reflection of the importance of the electrophoretic term (Equation 1) in the Lys/BSA case. However, there is a molecular-sieving contribution as well because in the Lys/BSA case we are attempting to separate a 14 kDa from a 67 kDa protein (ΔMW = 53 kDa) and in the CA/Hb case we are attempting to separate a 29 kDa from a 65 kDa protein (ΔMW = 36 kDa). The importance of the molecular-sieving contribution can be seen by comparing the Lys vs. CA fluxes in Figure 2-10 and Figure 2-11. For any nanotube ID, the flux of the larger CA molecule (Figure 2-11) is lower than the Lys flux (Figure 2-10).

Hb/BSA two-protein transport experiments

The final variable to be explored is the effect of solution pH. This is important because the solution pH determines the magnitude of the net charge on the protein and thus determines whether an electrophoretic contribution to transport will be extant. For example, at pH = 4.9, Hb is positively charged (pI = 7.0) whereas BSA has no net charge (pI = 4.9). A series of Hb/BSA permeation experiments was conducted at pH = 4.9 for a membrane with 60 nm ID nanotubes, with and without an applied transmembrane potential of +8 V. Because BSA has no net charge, its flux with and without applied potential was found to be the same (Figure 4-12 and Table 2-5). In contrast, because it is positively charged, the flux of Hb increased by a factor of 60 when +8 V was applied (Table 2-5). Furthermore, this is an interesting situation where application of the

transmembrane potential reverses the selectivity – with no applied potential $\alpha_{BSA/Hb} = 5.6$ (diffusive transport selectivity), but with applied potential $\alpha_{BSA/Hb} = 0.1$ or $\alpha_{Hb/BSA} = 10$ (electrophoretic transport selectivity). This occurs because the molecular sieving term (Equation 1) favors BSA transport but the electrophoretic term favors Hb transport.

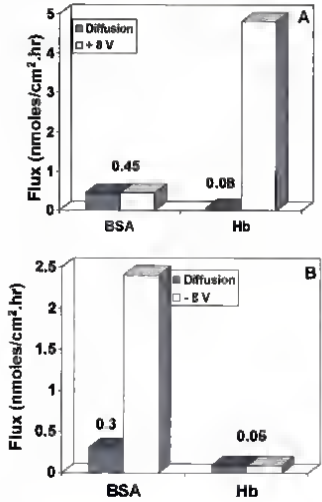

Figure 2-12. Diffusive and electrophoretic fluxes of BSA and Hb for two-protein permeation experiments at different pH under the applied potential. (A) At pH = 4.9 (isoelectric point of BSA) the applied potential is + 8 V. (B) At pH = 7.0 (isoelectric point of Hb) the applied potential is –8 V. Nanotube ID = 60 nm.

Because Hb and BSA have nearly the same molecular weight (65 vs. 67 kDa), the free-solution coefficients for both molecules are nearly the same (BSA, 5.9×10^{-7} cm^2 s^{-1}, [135] Hb, 6.4×10^{-7} cm^2 s^{-1}) [135] However, the diffusive flux of BSA in the membrane with 60 nm ID nanotubes is 5.6 times higher than that of Hb. Chun and Stroeve[116] also found that BSA diffuses faster than Hb in gold nanotube membranes. They have discussed various explanations for this observation including the possibility that it is related to difference in molecular shape, BSA is an elliptically-shaped molecule with approximate dimensions 4×4×14 nm,[121] whereas Hb is more spherical, with approximate dimensions of 6.4×5.5×5 nm.[136] A series of Hb/BSA permeation experiments was also conducted at pH = 7 for a membrane with 60 nm ID nanotubes, with and without an applied transmembrane potential of -8 V. Because Hb has no net charge at pH = 7, its flux with and without applied potential was found to be same (Table 2-5). In contrast, the flux of the charged BSA increased by a factor of 8 when -8 V was applied across the membrane. Again, the Hb/BSA selectivity is higher with applied potential ($\alpha_{BSA/Hb} = 26$) than without ($\alpha_{BSA/Hb} = 3$), but a reversal in selectivity is not observed. This is because in this case, the electrophoretic and molecular-sieving terms both favor BSA transport.

Table 2-5 Comparison of diffusive and electrophoretic fluxes of BSA and Hb for two-protein permeation experiments at pH = 4.9 (isoelectric point of BSA) and pH = 7.0 (isoelectric point of Hb). Nanotube ID = 60 nm.

	Flux (nmole hr^{-1} cm^{-2}) at pH = 4.9		Flux (nmole hr^{-1} cm^{-2}) at pH = 7	
	Diffusion	+ 8 V	Diffusion	- 8 V
BSA	0.45	0.45	0.3	2.4
Hb	0.08	4.8	0.09	0.09

Conclusions

These studies have shown that by controlling the IDs of the nanotubes, Au nanotube membranes can show good selectivity for separation of proteins on the basis of molecule size. In addition, by chemisorbing a PEG-thiol, the problem of membrane fouling by protein adsorption can be eliminated. Protein flux in these experiments was enhanced by applying a pressure difference across the membrane and by applying a potential across the membrane

Gold nanotube membranes are interesting model systems for exploring the flux-vs-selectivity tradeoff in membrane-based protein separations. In general, membranes containing larger ID nanotubes showed higher fluxes and lower selectivities than membranes with smaller ID nanotubes. This is the conventional flux-vs.-selectivity tradeoff. Transmembrane electrophoresis can, however, be used to optimize both flux and selectivity For example, for proteins that are oppositely charged, a combination of high transmembrane potential and large nanotube ID provides both high flux and excellent selectivity (Table 2-4)

Because the nanotubes have IDs that are larger than but comparable to the diameters of the protein molecules, hindered transport occurs within these membranes. This enhances the molecular-sieving component of the transport selectivity above what would be predicted based on the free-solution diffusion coefficient values. In addition, another type of hindered diffusion has been observed in which the flux of one protein molecule is hindered by the presence of a second protein molecule in the nanotube (Table 2-3) In addition to transmembrane potential and nanotube diameter, solution pH value plays an important role in determining the transport selectivity. This is because pH

determines the net charge on the protein molecule and this, in turn, determines whether electrophoretic transport is possible and, if so, in which direction

CHAPTER 3
NANO WHEAT FIELDS PREPARED BY PLASMA-ETCHING GOLD NANOWIRE-CONTAINING MEMBRANES

Introduction

The Martin group and others have been investigating a general method for preparing nanomaterials called template synthesis.[41, 43, 46, 64, 78, 86, 133, 137, 141] This method entails synthesis of a desired material within pores of a nanopore membrane or other porous solid. Depending on the membrane and synthetic method used, cylindrical nanostructures with monodisperse diameters and lengths are obtained, and may be solid nanowires or hollow nanotubes. Nanowires and tubes composed of metals,[78] polymers,[86, 137] semiconductors,[46] carbons,[133] and other materials[64, 138, 139] have been prepared. The ability to control the dimensions of the nanowires and tubes obtained is an important feature of the template method. Diameter can be controlled by varying the diameter of the pores in the template membrane. The lengths of the nanostructures can be controlled by varying the thickness of the template membrane. Alternatively, for electrochemical deposition within the pores, the length can be controlled by varying the deposition time.[41]

One application of template-synthesized nanowires that we are pursuing is as building blocks for self-assembly of supramolecular architectures.[86] For example, it has been shown that dithiol chemistry can be used to self-assemble colloidal Au nanoparticles onto the ends of template-synthesized Au nanowires.[86] Unfortunately, the efficiency of that process was low because the ends of the Au nanowires were recessed within the pores of the template membrane. In that research it was proposed that the efficiency of

the self-assembly process would be improved if a method that allowed the ends of the nanowires to protrude from the template membrane was employed. Such a method is described here. Because they are of interest to the self-assembly work, we illustrate this method with gold nanowires deposited within the pores of a polycarbonate template membrane.[78] A new approach is reported here for effectively controlling the lengths of template-synthesized nanostructures. We show that by exposing these membranes to an O_2 plasma, the polymer at the membrane surface is selectively removed, thus exposing the ends of the Au nanowires. The length of the exposed nanowires can be controlled at will by varying the plasma etching time. The protruding ends of the Au nanowires resemble wheat fields.

Experimental

The template membranes were track-etched polycarbonate filters obtained from Osmonics (Poretics). These membranes are 6 μm thick with nominal pore diameter and pore density of 30 nm and 6×10^8 pores cm^{-2}, respectively. The electroless Au plating procedure used to deposit the Au nanowires within the pores of these membranes has been described previously.[43,78] This method yields the Au nanowires within the pores as well as thin Au films that cover both faces of the membrane.[43,78] Both of the Au surface films were removed by simply applying and then removing a strip of Scotch tape.[43] The ends of the nanowires were then exposed by O_2-plasma etching the surface of the membrane using a Samco plasma reactive ion etching system (Model RIE-1C). The etching conditions were as follows: power = 100 W, oxygen pressure = 300 Pa, flow rate = 30 standard cm^3 min^{-1}.

The samples were imaged using a Hitachi S-4000 field emission scanning electron microscope (FESEM). The sample was attached to an SEM sample stub using a piece of double-coated copper foil tape. To improve the quality of the SEM, the surface assembly was then sputtered with a very thin layer of Au/Pd using a Desk II cold Sputter/Etch system.

Results and Discussion

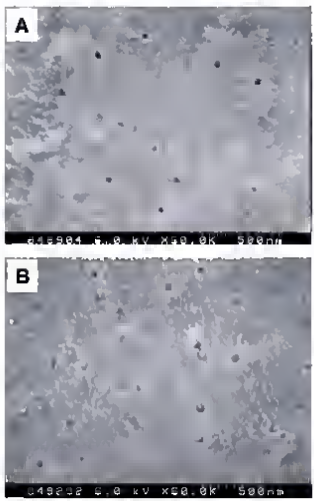

Figure 3-1. Scanning electron micrographs (SEMs) of the template membrane before (A) and after (B) electroless deposition of the Au nanowires. The image in B was obtained after removing the Au surface film.

Field emission scanning electron micrographs (FESEMs) of the membrane prior to electroless Au deposition (Figure 3-1A) show that the pores at the membrane surface are 32 ± 6 nm in diameter, in agreement with the nominal pore diameter specified by the vendor. After electroless deposition and removal of the Au surface films, the ends of the Au nanowires can be seen protruding from some of the pores (Figure 3-1B), however, the nanowire ends are clearly recessed in some cases. Whether the nanowire tip is recessed or protruding depends on where the nanowire broke when the Au surface film was removed. This was proven by imaging the surface of the Scotch tape used to remove the Au surface film (Figure 3-2). The excised nanowire ends, corresponding to the recessed pores in Figure 3-1B, are seen in such images.

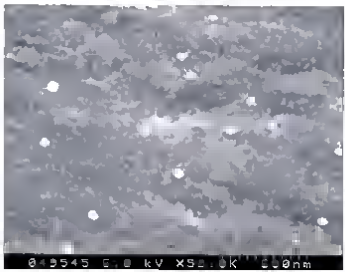

Figure 3-2. SEM image of the surface of the Scotch tape after using the tape to remove a Au surface film.

The O_2 plasma causes the polycarbonate at the membrane surface to be etched away, exposing the ends of the Au nanowires (Figure 3-3). The length of the exposed nanowires increases with etch time (Figure 3-4). While longer etch times result in further

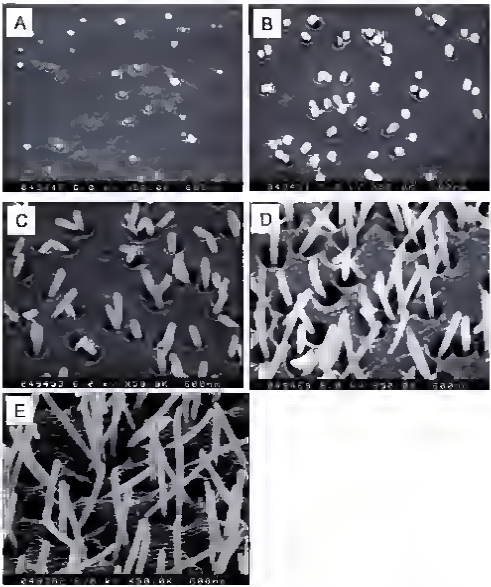

Figure 3-3 SEMs of the surfaces of membranes that were O_2-plasma etched for 5 (A), 10 (B), 30 (C), 60 (D) and 120 (E) seconds.

nanowire exposure, it is difficult to obtain the length because the exposed wires ultimately obscure the underlying membrane surface (Figure 3-5). A number of interesting features can be seen in the images in Figure 3-3. First, the surfaces of the Au nanowires are scalloped. We have observed analogous scalloping in template-

synthesized polypyrrole nanowires, and we showed that this occurs because the pore walls of the template membrane are also scalloped.[137] Second, as etch time increases, preferential etching of the membrane occurs around the "stalks" of the nanowires. This may result from plasma-induced heating of the nanowires, resulting in localized heating of the membrane around the stalks. Finally, at longer etch times, unidirectional "furrows" are seen in the polycarbonate surface (Figure 3-3 D and E). This undoubtedly occurs because these membranes are stretch-oriented during fabrication,[137] and the furrows are along the stretch direction.

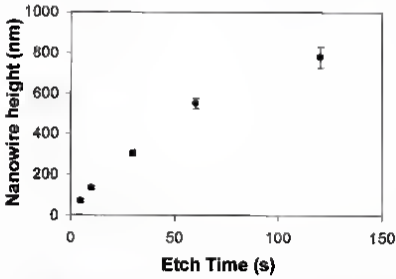

Figure 3-4 Plot of length of the plasma-exposed portion of the Au nanowires vs plasma etching time

The diameter of the exposed nanowire is always greater than the 32 nm pore diameter obtained from SEM images of the membrane surface. For example, the following average nanowire diameters were obtained at the indicated etching times: 63 ± 6 nm (5 s etch), 76 ± 7 nm (10 s etch), 70 ± 4 nm (120 s etch). It is now well established

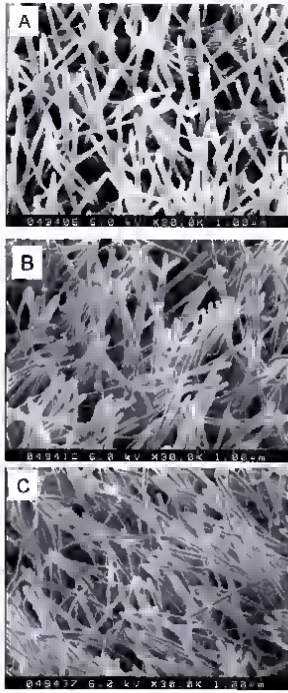

Figure 3-5. SEMs of the surfaces of membranes that were O_2-plasma etched for 180 (A) 240 (B), and 400 (C) seconds

that the pores in these membranes have conical tapers at the membrane surfaces; i.e., cigar-shaped pores.[78, 140, 141] The 32 nm diameter (measured from the surface images) corresponds to the diameter of the tip of the cigar-shaped pore. The ~ 70 nm nanowire diameter obtained for longer etching times corresponds to the diameter of the cylindrical part of the pore that runs through most of the membrane thickness.

We do not, however, see conical nanowire ends in our images; instead the ends look blunt. This is related to the issue of where the nanowire breaks when the Au surface layer is removed. Since, the conical end is the narrowest part of the nanowire, the wires break at this point more frequently. Hence, we believe that the conical part adheres primarily to the Scotch tape used to remove the Au surface layer. It is interesting to note, however, that the average nanowire diameter obtained after 5 s of etching (63 ± 6 nm) is smaller than the steady-state diameter obtained for long etch times (70 to 76 nm). This suggests that some part of the narrower conical section of the nanowire remains with the membrane after the Au surface layer is removed.

The longer etch time images (Figure 3-5) reveal another interesting feature of the plasma-etching process--the density of the nanowires (number of nanowires per cm^2 of membrane surface area) increases with etching time. This occurs because the membrane shrinks at longer etch times. This can be observed by simple visual inspection of the membrane before and after plasma treatment. For example, a piece of membrane that was 12 mm × 7 mm before etching was 10 mm × 4 mm after 3 min of plasma etching. We believe that shrinkage results from plasma-induced heating of the membrane because these membranes were shown previously that they can be shrunk by heating above the glass transition temperature of the membrane material.[43]

Conclusions

In conclusion, a new approach has been demonstrated for effectively controlling the length of template-synthesized nanowires. This method should be applicable in any case where the material composing the nanowires (or tubes) etches at a slower rate than the material making up the template membrane. In addition to using these exposed nanowire tips for self-assembly applications,[86] we are also using this method to improve electrical contact between nanowire-containing membranes and substrate metal surfaces. According to our observations, membranes with exposed Au nanowires show lower contact resistance values with a metal surface than membranes in which the nanowires have not been plasma etched.

CHAPTER 4
CONTROLLABLE AND ADDRESSABLE GLASS NANOWELLS FROM PLASMA ETCHING

Introduction

Nanotechnology is revolutionizing the electronic, chemical and biotechnology fields.[1] In contrast with the top-down manufacturing strategy used in industry, nanotechnology provides a bottom-up alternative. By building up new products from molecules and nanostructures, similar to the strategies of Mother Nature, it is possible to construct complex nanoscale architectures. Nanofabrication and nanopatterning are making it possible to develop diverse applications of nanostructured devices. Applications include those used in ultradense data storage, sub-wavelength optics, and nanoelectronics.[2,3] One of the key elements in the successful development of these devices is the ability and the flexibility to control nanostructure dimensions and surface patterning.

Different techniques have been used to produce the nanoscale size structures, such as electro-beam-writing and lithographic methods using deep UV, X-ray or electron beams.[142] These serial methods require sophisticated equipments, have high cost and pattern only small areas. Another limitation for these techniques is that they cannot be applied to unstable and bio-chemically functionalized surface layers. Soft lithography has been developed using polymer especially PDMS mask to produce nanostructures in combination with solution etching.[3,143-145] However, because of possible distortion

resulting from soft stamp, high resolution of nanostructure features is not easy to be obtained [146]

Ordered arrays of micrometer- and nanometer-sized wells were fabricated by chemically etching a distal face of a 1000-μm diameter optical imaging fiber with 30-, 15-, 3- and 0.3-μm lapping films [147] Well depth was controlled by the etching reaction time and the smallest wells had a 50-nm depth and a 250-nm diameter with very short etching time.

Atomic force microscopy (AFM) is a suitable technique for probing the chemical nature of surfaces.[148-151] By using the tip as a spring, the interaction force between a sharp tip and a flat surface of a specific material can be measured by monitoring the pull-off force required to return the tip to its equilibrium position.

In this work, a method was developed to produce highly ordered nanoarrays called nanowells by use of highly ordered alumina porous membrane as a mask and plasma etching technique. The depth of the nanowells was controllable by varying the etching time. Inside and outside of the nanowells can be relatively easier to be modified with different chemistry. In addition, the inside of the nanowells was modified with molecular linkers so that the concurrent linkage of nanoparticles was successfully attached. Currently, we are investigating the potential applications of such nanowells.

Experimental

Materials

Aluminum foil (100 × 500 × 0.5 mm, purity 99.99%, Alfa Aesar), microscope premium finest glass slides (75 × 25 × 1 mm, Fisher Scientific), silanes (structures shown in Figure 4-1) used for modification including triethoxysilylbutyraldehyde (aldehyde

silane, UCT), 3 aminopropyltriethoxysilane (APTS or aminosilane, Gelest), tetraethylorthosilicate (TEOS) and octadecyltrichlorosilane (OTS, Aldrich), anhydrous toluene (Sigma-Aldrich), Triton X-100 (Aldrich), hexylalcohol (Aldrich), cyclohexane (Fisher), NH_4OH (Fisher Scientific), acetone (Fisher Scientific), aldehyde/sulfate white polystyrene latex (43 ± 10 nm, Interfacial Dynamics Corporation), phosphate buffered saline (PBS buffer: Sigma-Aldrich), sodium chloride (Fisher Scientific)

A) 3-Aminopropyltriethoxysilane (APTS or aminosilane)

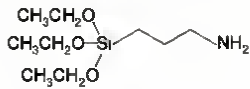

B) Triethoxysilylbutyraldehyde (aldehyde silane)

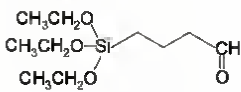

C) Octadecyltrichlorosilane (OTS)

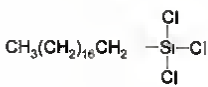

D) Tetraethylorthosilicate (TEOS)

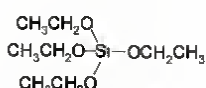

Figure 4-1. Structures of silanes used for modification.

Preparation of the Nanopore Alumina Membrane

Masuda's two-step method was used for preparing high quality nanopore alumina membrane.[19] As mentioned somewhere else,[152] 1.2 μm thick alumina nanopore

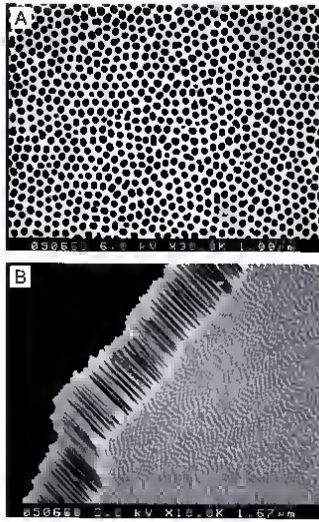

Figure 4-2 Scanning electron micrographs of alumina membrane (A) Top view of homegrown 80 nm. (B) Side view of the membrane

membrane has been produced by anodization of aluminum. Briefly, the Al foil was first degreased using acetone and then annealed in air at 400 °C for 1 h. A 42 cm^2 section of foil was then electropolished at 15 V in a solution that was 95 wt % H_3PO_4, 5 wt %

H_2SO_4, and 0 20 M in CrO_3 using a Pb plate as cathode After rinsing with distilled water, the polished Al foil was anodized at 50 V in 5 wt % aqueous oxalic acid at 1 5 °C for 1 h, the cathode was a stainless steel plate This resulted in the formation of thin nanopore alumina film on the surface of the Al foil. The precursor film was dissolved away in an aqueous solution of 0 2 M in CrO_3 and 0 4 M in H_3PO_4 at 80°C. As discussed by Masuda,[19] this leaves a highly ordered pattern of scallops on the Al substrate.

In the second step this textured Al substrate was anodized for 15 min at 50 V in the 5 wt % oxalic acid solution. This yields the desired ordered nanopore alumina film. Figure 4-2 shows the top view and side view of homegrown 80 nm alumina nanopore membrane used in this work. Voltage reduction technique was then used to detach this film from the underlying Al surface This entails gradually (over a period of 1 h) reducing the anodizing voltage from 50 V to 15 V, followed by film detachment by immersing in 10 wt % H_3PO_4 solution. The resulting free-standing nanopore alumina membrane (1 2 μm thick) has two distinct surfaces, the barrier layer surface, which faces the substrate Al foil during the anodization process, and the solution surface

Fabrication of Nanowells

Nanowells of glass were obtained by an argon plasma etching method using the alumina nanopore membranes as masks Glass slides were sequentially cleaned in 20 % sulfuric acid, DI water, ethanol, and then DI water before etching Figure 4-3 is schematic of glass etching process by argon plasma. A piece of alumina nanopore membrane was placed, with barrier layer surface up on top of a glass slide. The assembly was then inserted into the center of the vacuum chamber of a reactive ion etching apparatus (Samco Plasma Ion Etching System, model RIE-1C) The etching

conditions were as follows: power = 140 W, argon pressure = 10 Pa, flow rate is 9 standard cm^3 min^{-1}

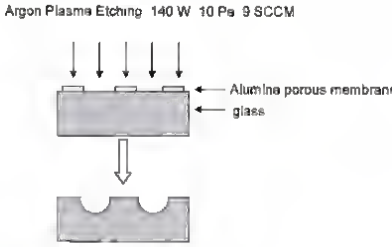

Figure 4-3 Glass etching process by argon plasma.

Atomic Force Microscopy (AFM)

AFM studies were performed using a Multimode NanoScope IIIa AFM (Digital Instruments). For enhanced resolution, oxide-sharpened SSS tips (super sharp silicon tips, Nanosensors) were used for tapping mode imaging. Image density of 512 x 512 pixels and scan rate of 1 Hz were usually used. A 10 um tube scanner was used to obtain topography and friction measurements.

All friction imaging and measurements were performed at contact mode using LFM tips (Nanosensors) under dry N_2 gas in an environmental chamber (Digital Instruments).

The normal force between the tip and sample, F_N, was estimated using the sprung constant provided by manufacturer and tip deflection sensitivity obtained from tip deflection vs. z-displacement curves. All of the frictional measurements and images were

obtained with the fast scan axis perpendicular to the principal axis of the cantilever. Slow scan axis was disabled to ensure the same area sampled.

Friction forces, f, were calculated from plots of frictional signal vs. lateral displacements during 250 nm trace/retrace cycles--friction loops along a single scan line repeatedly back and forth at 1000 nm/s. Friction forces were measured as a function of systematically varying F_N. At least 10 measurements of friction forces were acquired for each F_N.

For good comparison, all friction data were obtained using the same tip throughout the experiments. The LFM tip was washed in methanol prior to each measurement. Thus, variables such as the cantilever force constant and tip structure were fixed. To verify the tip composition during repeated measurements, a bare glass sample was used. Identical results were obtained for a bare glass sample before and after characterizing other samples.

Silica Nanoparticle Synthesis and Characterization

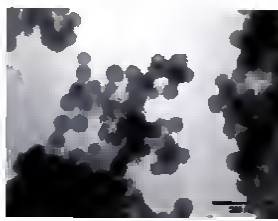

Figure 4-4. TEM image of the silica nanoparticles.

Pure silica nanoparticles were synthesized by the Stoeber synthesis.[153-155] Synthesis was via water-in-oil microemulsion (Triton X-100/cyclohexane/n-

hexanol/water) technique. TEOS was added to the microemulsion and hydrolyzed for the silica synthesis, and NH_4OH was added as a morphological catalyst. Then the nanoparticles were isolated from microemulsion with acetone. Silica nanoparticles have been characterized by a Hitachi transmission electron microscope, model H7000. In this work, the sizes of the silica nanoparticles used are 65 ± 5 nm, as shown in Figure 4-4.

Chemical Modification Inside and Outside of the Nanowells

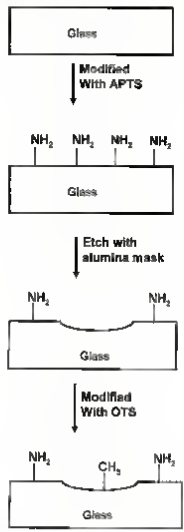

Figure 4-5. Different modification inside and outside of the nanowells.

One way to modify inside and outside of the nanowells with different chemistry is to attach different silanes via silanization. In an example as shown in Figure 4-5, the first silane–aminosilane was attached on a piece of clean glass in a solution of 5% silane in 90% ethanol and 5% NaAc/HAc (50 mM, pH 5.2) solution for 20 min. This silane monolayer on glass was cured in oven (120 °C) for 2 hours. After thoroughly rinsing, the modified glass with the monolayer was then etched for 30 s with a piece of nanopore alumina membrane as a mask with the barrier layer up. After etching, the etched modified glass was immersed into the second silane solution (1% OTS in toluene) for 10 min. In this way, aminosilane is outside the nanowells, while OTS is inside the nanowells.

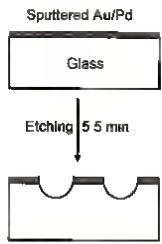

Figure 4-6 Nanowell etching process from Au/Pd sputtered glass.

Another way to modify inside and outside the nanowells with different chemistry is to deposit or sputter a thin layer of appropriate material on glass surface before etching. For example, this can be done by sputtering down Au/Pd thin layer or depositing carbon layer by chemical vapor deposition (CVD). After etching the substrate, the inside of the nanowells is easily modified by silanization, while the outside of the nanowells can be

modified by the corresponding chemistry from the deposited thin layer of other material (e.g , Au-thiol chemistry for Au/Pd thin layer) If a further modification is wanted, a silane can be used as a molecular linker to link other molecules or modified nanoparticles to the regions. The following part will describe how to selectively attach the silica nanoparticles inside the nanowells The strategy used here is to protect outside of the nanowells from silanization by sputtering a thin layer of Au/Pd before etching The resulted nanowells etched from Au/Pd sputtered glass are shown in Figure 4-6 The surface of the clean glass was sputtered with Au/Pd (~ 20 nm thick) by using a Desk II cold sputter/etch system (Denton Vacuum, LLC) A piece of alumina porous membrane with pore size of ~ 80 nm was put on the sputtered glass with the barrier layer surface up The glass surface was exposed by etching away Au/Pd through alumina membranes pores. Inside the nanowells is the exposed glass surface, while outside of the nanowells is Au/Pd surface which can prevent silanization.

Selective Attachment of Nanoparticles

There are two types of nanoparticles selectively attached into the nanowells. One type is silica nanoparticles, the other type is aldehyde modified white polystyrene latex nanoparticles

Silica nanoparticle attachment

The resulted etched substrate from Figure 4-6 was immersed into 5% aldehyde silane (molecular linker **1**) in 90% ethanol and 5% NaAc/HAc (50mM, pH 5.2) for 20 min at room temperature under Ar or N_2 atmosphere The substrate was then rinsed with ethanol, and cured under nitrogen for overnight As a result, the glass surface inside the nanowells was modified with a monolayer of the aldehyde silane

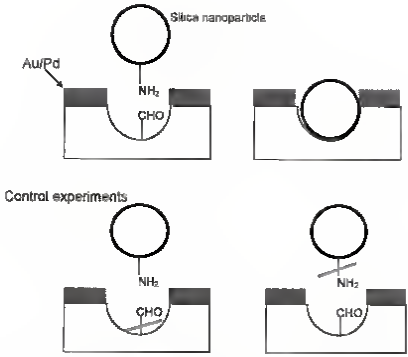

Figure 4-7 Procedure of attaching silica nanoparticles into the nanowells and the control experiments.

Silanization of silica nanoparticles were performed by immersing in freshly prepared 5% aminosilane (molecular linker 2) in 90% ethanol and 5% NaAc/HAc (50 mM, pH 5.2) solution for 20 min. The modified silica nanoparticles together with the solution were microcentrifuged with an Eppendorf 5417C microcentrifuge at 14500 rpm for 10 min to remove excess of aminosilane. The modified silica nanoparticles were thoroughly rinsed with ethanol, water, phosphate buffered saline (PBS) solution (silica nanoparticles needed to be centrifuged). The modified silica nanoparticles were then dispersed into PBS solution. Finally, the aldehyde-modified substrate was immersed into the solution containing the dispersed aminosilane-modified silica nanoparticles, and incubated under nitrogen atmosphere with stirring for a few hours. The silica nanoparticles were connected to the nanowells via a linkage between the two molecular

linkers--the aldehyde and amine functional groups. The resulting substrate was washed with PBS and deionized water. For comparison, control experiments were done by neglecting one of the molecular linkers so that there is no chemistry happened between silica nanoparticles and nanowells. Figure 4-7 shows the procedure of attaching silica nanoparticles into the nanowells and comparison of control experiments.

Polystyrene nanoparticle attachment

Polystyrene latex nanoparticles modified with aldehyde/sulfate are commercially available. After the etched nanowells were obtained from plasma etching of Au/Pd sputtered glass, the substrate was immersed into 5% aminosilane in 90% ethanol and 5% NaAc/HAc (50 mM, pH 5.2) for 20 min. Aminosilane monolayer covered only inside the nanowells which is glass surface exposed by etching process. Then the amino-modified nanowell pattern was immersed into 10 mM NaCl containing well-dispersed polystyrene latex nanoparticles for 2 hours under nitrogen atmosphere, followed by rinsing in NaCl and DI water.

Results and Discussion

Depth of the Etched Nanowells

A series of nanowell array were prepared under the etching conditions mentioned above, varying only the etching time. From the SEM images (not shown here), we can tell that the contrast is higher with longer etching time, which suggests that longer etching time resulted in deeper nanowells. Since depth can not be accurately determined from SEM images, AFM was turned to be an alternative way to obtain the depth of the nanowells.

A series of 500 nm x 500 nm AFM images (Figure 4-8) were obtained with different etching time. Figure 4-9A shows the change in cross-sectional profiles derived

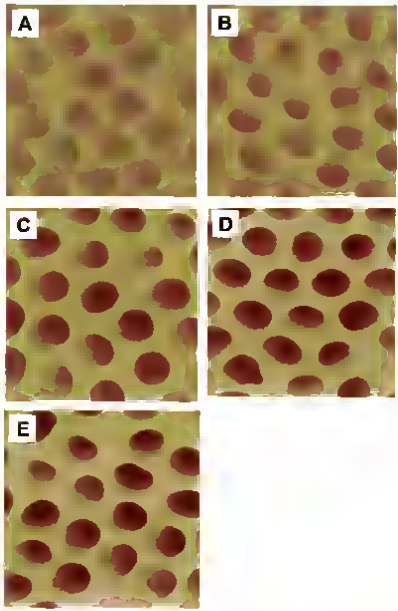

Figure 4-8 500 nm x 500 nm AFM images of etched glass at different etching time Etching times are 1 (A), 2 (B) 3 (C), 4 (D) and 5 (E) minutes, respectively

from the AFM images as a function of etching time. Each curve is a representative profile of one nanowell for each etching time More than 50 nanowells were measured at each etching time and a plot of etching depth-vs -etching time was obtained, as showe in

Figure 4-9B An etching time of 1 min resulted in around 4 nm deep nanowells Increasing the etching time resulted in deeper nanowells 5 min etching can result in nanowells approximately 18 nm in depth.

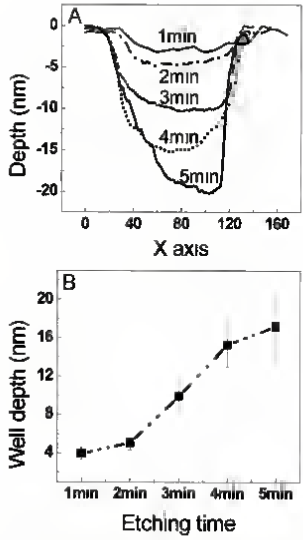

Figure 4-9 Depth measurements of the nanowells Cross-sectional profiles of single nanowell derived from the AFM images as a function of etching time (A) Depth of nanowells vs etching time (B)

Selective Attachment of Nanoparticles

After Au/Pd sputtering the glass was etched using the alumina porous membrane as a mask, with barrier layer surface up, for 5.5 min. According to our observation, 0.5 min is long enough to remove the sputtered Au/Pd layer completely without alumina mask. Etching time 5.5 min was chosen in Figure 4-6 because that is enough to expose glass surface underneath the Au-Pd layer and to obtain deep enough nanowells to hold nanoparticles for the following selective attachment. Figure 4-10 shows AFM image of

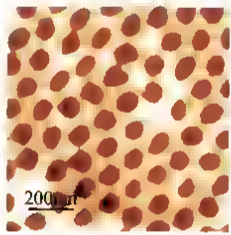

Figure 4-10 AFM image of the resulted nanowells etched from Au/Pd sputtered glass Tapping mode

resulted nanowells from etching. The resulted nanopatterns are very uniform and highly ordered. Inside the nanowells is exposed glass surface, while outside the nanowells is still Au/Pd surface. The method is applicable to sputter or deposit other materials for example carbon on the substrate. Etching will automatically create surfaces of different materials which are suitable to be modified based on the appropriate chemistry.

Silica nanoparticle attachment

In order to selectively attach the silica nanoparticles inside the nanowells, the inside of the nanowells was modified with an aldehyde-terminated molecular linker, and the

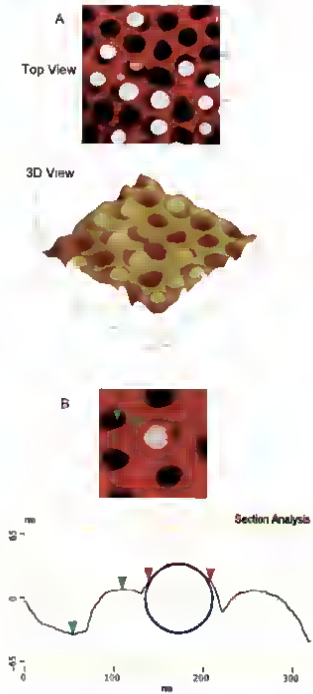

Figure 4-11 Selective attachment of silica nanoparticles into nanowells (A) AFM images (B) Section analysis.

silica nanoparticles were modified with an amine terminated molecular linker. When the amine groups on the silica nanoparticles met aldehyde groups inside the nanowells, reaction between them resulted in the linking of nanoparticles to the nanowells. Figure 4-11A shows the AFM images of selective attachement of silica nanoparticles in the nanowells. Cross-section analysis of the image was conducted by crossing one empty nanowell and one nanowell filled with silica nanoparticles as displayed in Figure 4-11B.

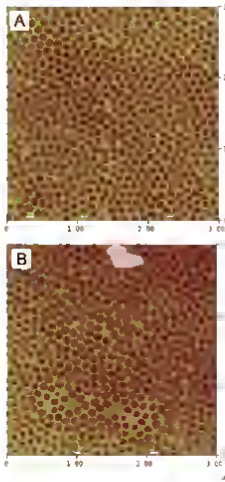

Figure 4-12 AFM images of control experiments by neglecting one of the silanes (A) Neglect aldehyde silane on the glass surface (B) Neglect aminosilane on silica nanoparticles Tapping mode

The distance between the green cursors is 45 9 nm which is the depth of the nanowells, this depth is much larger than the expected value from etching the glass (~18 nm for 5 min etching as shown in Figure 4-9B) The sputtered layer is around 20 nm in thickness, which can be etched away only within 30 s, the resulted depth here is the sum of Au/Pd layer and the etched glass. From Figure 4-11, the nanoparticle diameter of 69 nm is consistent with the measurements of nanoparticles from TEM image (Figure 4-4). Control experiments were conducted by neglecting either the aminosilane or the aldehyde silane, and no nanoparticles was observed to attach to the inside of the nanowells as shown in Figure 4-12. This further confirmed that nanoparticles inside the nanowells in Figure 4-11 resulted from the linking between the amine and aldehyde functional groups

Polystyrene nanoparticle attachment

When aminosilane modified nanowells were immersed into 10 mM NaCl solution containing well-dispersed aldehyde modified polystyrene nanoparticles, the $-NH_2$ and –CHO functional groups reacted. As a result, the polystyrene nanoparticles were attached to the inside of the nanowells. Figure 4-13 shows AFM image of selective attachment of aldehyde–modified polystyrene nanoparticles into the nanowells. Control experiments were investigated as well The exposed glass surface inside the nanowells could have some charges induced by plasma etching, while the aldehyde modified polystyrene nanoparticles are negatively charged In order to avoid electrostatic interaction between them, in the control experiments, the exposed glass surface was modified with OTS, there were no polystyrene nanoparticle attached to the inside of the nanowells. We also tried to immerse glass slide and Au/Pd sputtered substrate into the NaCl solution containing polystyrene nanoparticles, no attachment was observed either. All these control

experiments confirmed that the polystyrene nanoparticles inside the nanowells in Figure 4-13 were caused by interaction between amino groups and aldehyde groups

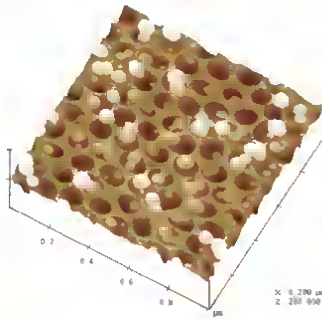

Figure 4-13 AFM image of polystyrene nanoparticle selective attachment into the nanowells. Tapping mode

Friction Measurements with AFM

Atomic force microscopy (AFM) is a suitable technique for measurement of surface forces (attraction/repulsion) between a tip and a surface of specific material, therefore, it was used here to measure the different surface forces between the tip and the different monolayers.

Friction forces of different chemical modification substrates were measured as a function of systematically varying F_N using the same AFM tip. The substrates were modified with APTS and OTS having $-NH_2$ and $-CH_3$ end groups, respectively. Friction forces, f, were measured from plots of frictional signal vs. lateral displacements during 250 nm trace/retrace cycles--friction loops along a single scan line at 1000 nm/s. Figure

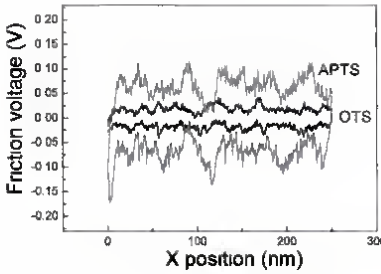

Figure 4-14 Plots of frictional signal vs lateral displacements during 250 nm trace/retrace cycles along a single scan line at 1000 nm/s. Applied load = 20 nN Grey curve–APTS modified surface. Black curve–OTS modified surface

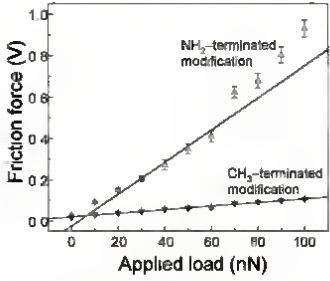

Figure 4-15 Friction forces as a function of applied loads for modified surfaces with different chemistry

4-14 indicates plots of frictional signal vs lateral displacements at 20 nN applied load. The flat and unetched glass was modified with either APTS or OTS. The upper curve for each modified surface is corresponding to trace scan, and the lower one is retrace scan. 90% of the curve in the middle was taken for calculation of friction force. The difference between trace and retrace average values was the friction force at an applied force of 20 nN. Then, friction forces were measured as a function of systematically varying F_N. At least 10 measurements of friction forces were acquired for each F_N. Figure 4-15 shows the friction forces as a function of applied loads for modified surfaces with different chemistry. For both modified surfaces, friction force, f, exhibits linear dependence on applied load–F_N that can be described by

$$f = \alpha F_N + f_0$$

where α and f_0 are constants that are related to the chemical composition of the interface.[156] The values of α and f_0 are influenced by the chemical identity of the end groups of the organic monolayer. APTS modified regions whose end groups–amine groups was hydrophilic have a higher friction force with hydrophilic AFM tip than OTS modified regions with hydrophobic terminal methyl groups. Friction force is also a function of the surface free energy. That is, the higher the surface free energy, the greater measured friction. Tha regions with terminal amine groups has higher surface free energy than that with terminal methyl groups, as reflected by larger contact angle of NH_2–terminated regions. Therefore, at same applied load, APTS modified regions have larger friction forces.

Besides putting nanoparticles inside the nanowells, different chemistry inside and outside of the nanowells was also investigated. Different monolayers are modified on the

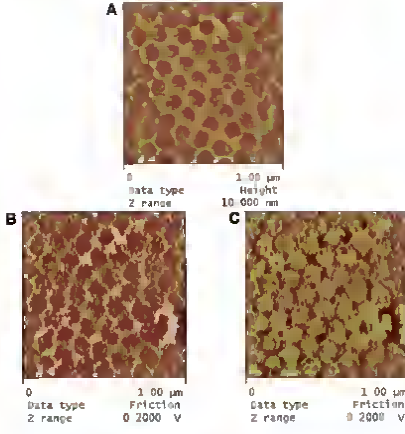

Figure 4-16 AFM height and friction images when NH_2–terminated molecules are outside the nanowells and CH_3–terminated ones are inside the nanowells (A) Top view of the height image (B) Top view of the friction trace image. (C) Top view of retrace image Applied load = 20 nN Contact mode.

different regions of the nanowells According to our observations, 10 s is long enough to etch away the monolayers without an alumina mask Therefore, for AFM friction measurements, etching time 30 s was carried out to open the barrier layer of the porous alumina membrane and to etch away the monolayer exposed to the plasma etching Figure 4-16 shows the AFM height and friction images when NH_2-terminated molecules are outside of the nanowells and CH_3-terminated ones are inside of the nanowells as shown in Figure 4-5 Figure 4-16A indicates height image of resulted nanowells from 30

s etching In friction trace and retrace images as shown in Figure 4-16B&C respectively, the contrast difference shows the interaction difference between the AFM tip and the functional groups on the substrate Dark areas in friction images correspond to low frictions. The regions of high friction force arise from contact of the tip with terminal amine groups of APTS, and the regions of low friction force correspond to contact with the terminal methyl groups of OTS Figure 4-17 shows the corresponded height

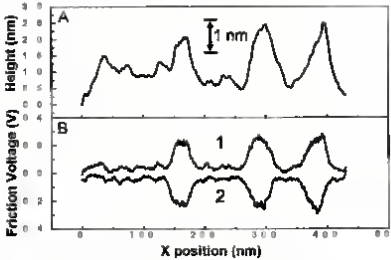

Figure 4-17 The corresponded height and friction force measurements to Figure 4-16 (A) Height measurement. (B1) Friction trace data. (B2) Friction retrace data.

measurement and friction force measurement expressed as friction voltage between the modified monolayer and the AFM tip The depth of the nanowells is only ~ 1 5nm, and even with so short etching time, the resulted nanowells are still highly ordered. According to the modification procedure (Figure 4-5), inside the nanowells are CH_3– terminated molecules, and outside the nanowells are NH_2–terminated molecules. Since the AFM tip is hydrophilic, the hydrophilic $–NH_2$ end groups have higher friction with AFM tip than hydrophobic $–CH_3$ end groups. Higher parts on the height curve (outside

the nanowells) are corresponding to larger friction force on friction voltage curve Compared to the height image in Figure 4-16A, the friction image is less ordered. That is because part of the NH_2-terminated monolayer covered by the membrane is etched away which could come from infirm attachment between the monolayer and the membrane mask.

Conclusions

In this work, highly ordered alumina membranes were used as masks to etch glass to obtain arrays of nanowells. This method has the ability to control the dimensions of nanostructures and the flexibility to pattern surfaces. The depth of the nanowells can be controlled by changing the etching time. Inside and outside of the nanowells can be modified with different chemistry. In addition, after the nanowells were modified with molecular linkers, the concurrent nanoparticles modified with corresponding molecular linkers were selectively attached to the specific location.

Atomic force microscopy (AFM) was used to characterize the nanopatterns and obtain the depth of the etched nanowells. Friction measurements can be conducted to obtain the friction force difference between different functional groups and AFM tip. Surface with higher free surface energy resulted in larger friction forces at same applied load. For both APTS and OTS modified surface, friction force exhibited linear dependence on the applied loads.

In this group, different pore sizes of alumina porous membranes have been grown. Pore sizes of alumina membranes can be controlled by adjusting voltage, pH, and different electrolyte solution.[10-15] By using various pore sizes of membranes as masks, the diameters of the etched nanowells can be controlled. Therefore, the diameters of

nanowells are controllable as well The etching method can be applicable to other substrates for example mica.

The specific modification of molecules can be used to detect the corresponding molecules. For example, the nanowells are modified with DNA which acts as a molecular anchor, and then the following complimentary DNA with specific marker can be detected

Another possible application is the nanowire fabrication by using the resulted nanowells as a template Nanowires can be grown inside the nanowells by electroless plating or electrical deposition. Since the diameter and the depth of the nanowells can be varied at will by using different pore sizes of alumina mask and changing etching time, nanowires with variable diameter, variable length and even variable materials can be obtained by using the etched nanowells as templates

CHAPTER 5
CONCLUSIONS

The objective of this dissertation is to produce nanostructures with controllable dimensions and to investigate the potential applications in chemical separations and sensors. Membrane-based synthesis is a concise and general method for preparation of nanomaterials. Chapter 1 introduces the background information of this research. It outlines how the gold nanotube and nanowire membranes are prepared from membrane template synthesis, and their applications that have been investigated. Plasma etching technique is also explained in Chapter 1 as it is used in subsequent chapters.

Chapters 2 and 3 involve the use of polycarbonate track-etched (PCTE) membranes as templates for the preparation of nanotubes or nanowires. The sizes of the nanostructures depend on the pore sizes of PCTE. Because the pores of PCTE membranes are monodisperse, the resulting nanotubes and nanowires show an analogous monodispersity.

In Chapter 2, template-based template synthesis is used to prepare gold nanotube membranes via electroless gold plating. The pore sizes of the gold nanotube membranes are controlled by changing plating time and using different pore sizes of template PCTE membranes. Because of the stable gold-thiol chemistry, the membranes can be easily modified with poly(ethylene glycol) to prevent protein adsorption on the membrane. The ability of avoiding membrane fouling is very advantageous since membrane fouling is a serious problem for membrane ultrafiltration. The applications of these engineered gold nanotube membranes in protein separations have been investigated. The membranes

have narrow pore size distribution and controllable pore size, therefore they show high selectivity to separate proteins. Because of the low transport rate resulting from nanopore size, two types of driving forces are applied to increase transport flux--transmembrane pressure and transmembrane potential. In transmembrane pressure applied method, protein separations are based on molecular size, and size-sieving effect on protein transport has been studied. Smaller pore size of membranes show higher selectivity to separate proteins, but the price is to have less productivity. In transmembrane potential method, size-sieving, charge and pH effects have been investigated on protein separations. Due to the ability of controllable pore sizes, gold nanotube membranes are interesting model systems for exploring the flux-vs -selectivity tradeoff in membrane-based protein separations. Electrophoresis can optimize the flux and selectivity. When the separated proteins have opposite charges, potential applied can beat the selectivity-vs.-flux tradeoff. However, when the separated proteins have same charges, small pore sizes of the membranes are necessary to obtain high selectivity. Buffer pH is very important in transmembrane potential applied method since it determines whether there is an electrophoretic transport, and if so, in which direction.

Chapter 3 describes the method developed to increase the efficiency of gold nanowires as building blocks for supramolecular architecture. The nanowires are synthesized via electroless gold plating as well. After the gold surface on the membrane is removed, there are separately standing nanowires within template membrane. These nanowires can be used as building blocks for self-assembly supramolecular architecture. But the efficiency is low because some of the nanowire ends are recessed within the template in some cases. Oxygen plasma etching has been used to selectively remove

surface layer of the polymer template and leave nanowire ends exposed. By adjusting the etching time, the length of the protruding nanowires can be controlled. Longer etching time results in high density of the protruding nanowires, which is due to the shrinkage of the polymer template. We believe the shrinkage results from plasma-induced heating of the membrane. Besides high efficiency as building blocks, these protruding nanowires can be used to increase electrical contact between the nanowire containing membrane and a substrate metal surface.

In Chapter 4, highly ordered alumina membranes are used as masks to etch substrates such as glass to obtain arrays of nanowells. The depth of the nanowells can be controlled by varying the etching time. Atomic force microscopy (AFM) is used to characterize the nanopatterns and obtain the depth of the etched nanowells. Inside and outside of the nanowells can be modified with different chemistry such as hydrophilic and hydrophobic functional groups. For example, NH_2-terminated and CH_3-terminated molecules are attached to the outside of the nanowells and the inside the nanowells, respectively. Friction measurements have been conducted to obtain the friction difference between the functional groups and AFM tip. The friction difference shows the interaction difference between the AFM tip and the functional groups on the substrate. Since the AFM tip is hydrophilic, the hydrophilic -NH_2 terminal groups have larger friction with AFM tip than hydrophobic -CH_3 terminal group. Also, friction force is a function of free surface energy, therefore, APTS modified surface with higher free surface energy has larger friction force than OTS modified surface. In addition, after the nanowells are modified with molecular linkers, the concurrent nanoparticles such as silica

or polystyrene nanoparticles modified with corresponding molecular linkers can be selectively attached to the specific locations

LIST OF REFERENCES

1 Dagni, R. *Chemical & Engineering News* **2000**, Oct 16

2. Markin, C. A.; Rogers, J. A. *MRS Bulletin* **2001**, *26*, 506-509

3 Odom, T. W.; Thalladi, V. R.; Love, J. C.; Whitesides, G. M. *J. Am. Chem. Soc.* **2002**, *124* 12112-12113.

4 Martin, C. R. *Science* **1994**, *266*, 1961-1966.

5 Hulteen, J. C.; Martin, C. R. *J. Mater. Chem.* **1997**, *7*, 1075-1087

6 Martin, C. R.; Mitchell, D. T. *Anal. Chem.* **1998** *70*, 322A-327A.

7 Chakarvarti, S. K.; Vetter, J. *Radiation Measurements* **1998** *29*, 149-159

8 Martin, C. R. *Chem. Mater.* **1996** *8*, 1739-1746

9 Fleisher, R. L.; Price, P. B.; Walker, R. M. *Nuclear Tracks in Solids*; University of California Press: Berkeley, CA, 1975

10 Bo, L.; Li, W. S. *J. Phys. D Appl. Phys.* **2000**, *33*, 2527-2531

11 Furneaux, R. C.; Rigby, W. R.; Davidson, A. P. *Nature* **1989** *337*, 147-149

12 Jessensky, O.; Mueller, F.; Goesele, U. *Appl. Phys. Lett.* **1998** *72*, 1173-1175

13 Li, A. P.; Mueller, F.; Birner, A.; Nielsch, K.; Goesele, U. *Adv. Mater.* **1999** *11*, 483-487

14 Masuda, H.; Hasegwa, F.; Ono, S. *J. Electrochem. Soc.* **1997** *144* L127-L130.

15 Smith, A. W. In *US Patent*; 3850762, 1974

16 Thompson, G. E.; Wood, G. C. *Treatise on Material Science & Technology*, Academic Press: NY, 1983

17 Thompson, G. E. *Thin Solid Films* **1997** *297* 192-201

18 Yakovlev, N. M.; Yakovlev, A. N.; Chupakhina, E. A. *Thin Solid Films* **2008** *366* 37-42.

19 Masuda, H.; Satoh, M. *Japan. J Appl phys Part 1* **1996,** *35*, L126-L129.

20 Tonucci, R. J., Justus, B. L., Campillo, A. J., Ford, C. E. *Science* **1992,** *258*, 783-785

21 Beck, J. S., Vartuli, J. C., Roth, W. J., Leonowicz, M. E., Kresge, C. T., Schmitt, K. D., Chu, C. T.-W., Olson, D. H., Sheppard, E. W., McCullen, S. B., Higgins, J. B., Schlenker, J. L. *J Am. Chem. Soc* **1992,** *114*, 10834.

22 Clark, T. D., Ghadiri, M. R. *J Am. Chem Soc* **1995,** *117*, 12364.

23 Douglas, K., Devaud, G., Clark, N. A. *Science* **1992,** *257*, 642

24 Ballarin, B., Facchini, M., Dal Pozzo, L., Martini, C. *Electrochem Commun* **2003** *5*, 625 631

25 Cai, Z., Martin, C. R. *J Am. Chem. Soc* **1989,** *111*, 4138-4139

26 Cai, Z., Lei, J., Liang, W., Menon, V., Martin, C. R. *Chem Mater* **1991,** *3*, 960-967

27 Liang, W., Martin, C. R. *J Am. Chem. Soc* **1990,** *112*, 9666-9668

28 Martin, C. R. *Adv Mater* **1991**, *3*, 457-459

29 Martin, C. R.; Parthasarathy, R. V. *Adv Mater* **1995** 7, 487-488

30 Parthasarathy, R.; Martin, C. R. *Nature* **1994,** *369*, 298-301.

31 Parthasarathy, R. V., Martin, C. R. *J Appl Polym. Sci.* **1996,** *62*, 875-886

32 Penner, R. M., Martin, C. R. *J Electrochem. Soc* **1986**, *133*, 2206-2207.

33 Van Dyke, L. S., Martin, C. R. *Langmuir* **1990,** *6*, 1118-1123.

34 Brumlik, C. J., Martin, C. R. *J Am. Chem Soc* **1991**, *113*, 3174-3175

35 Brumlik, C. J., Martin, C. R., Tokuda, K. *Anal Chem.* **1992,** *64*, 1201-1203

36 Brumlik, C. J., Menon, V. P., Martin, C. R. *J Mater Res.* **1994,** *9*, 1174-1183

37 Foss, C. A., Jr., Hornyak, G. L., Stockert, J. A., Martin, C. R. *J Phys. Chem.* **1992,** *96*, 7497-7499

38 Foss, C. A., Jr., Hornyak, G. L., Stockert, J. A., Martin, C. R. *Adv Mater* **1993**, *5*, 135-136.

39 Foss, C. A., Jr., Hornyak, G. L., Stockert, J. A., Martin, C. R. *J Phys. Chem.* **1994,** *98*, 2963-2971

40 Hornyak, G. L., Martin, C. R. *Thin Solid Films* **1997**, *303*, 84-88.

41 Hornyak, G. L., Patrissi, C. J., Martin, C. R. *J. Phys. Chem. B* **1997**, *101*, 1548-1555.

42 Hulteen, J. C.; Menon, V. P.; Martin, C. R. *J. Chem. Soc. Faraday Transactions* **1996**, *92*, 4029-4032.

43 Menon, V. P.; Martin, C. R. *Anal. Chem.* **1995**, *67*, 1920-1928.

44 Nishizawa, M.; Menon, V. P.; Martin, C. R. *Science* **1995**, *268*, 700-702.

45 Penner, R. M.; Martin, C. R. *Anal. Chem.* **1987**, *59*, 2625-2630.

46 Lakshmi, B. B.; Dorhout, P. K.; Martin, C. R. *Chem. Mater.* **1997**, *9*, 857-862.

47 Klein, J. D.; Herrick, R. D.; II, Palmer, D.; Sailor, M. J.; Brumlik, C. J.; Martin, C. R. *Chem. Mater.* **1993**, *5*, 902-904.

48 Parthasarathy, R. V.; Phani, K. L. N.; Martin, C. R. *Adv. Mater.* **1995**, *7*, 896-897.

49 Che, G.; Lakshmi, B. B.; Fisher, E. R.; Martin, C. R. *Nature* **1998**, *393*, 346-349.

50 Bowes, C. L.; Malek, A.; Ozin, G. A. *Chem. Vap. Deposition* **1996**, *2*, 97-103.

51 Shelimov, K. B.; Moskovits, M. *Chem. Mater.* **2000**, *12*, 250-254.

52. Blondel, A., Meier, J. P., Doudin, B., Ansermet, J.-P. *Appl. Phys. Lett.* **1994**, *65*, 3019-3021.

53 Schwarzacher, W. *Electrochem. Soc. Interface* **1999**, *8*, 20-24.

54 Ang, L.-M.; Hor, T. S. A.; Xu, G.-Q.; Tung, C.-H.; Zhao, S.; Wang, J. L. S. *Chem. Mater.* **1999**, *11*, 2115-2118.

55 Cepak, V. M.; Martin, C. R. *Chem. Mater.* **1999**, *11*, 1363-1367.

56 Patrissi, C. J.; Martin, C. R. *J. Electrochem. Soc.* **1999**, *146*, 3176-3180.

57 Miller, S. A.; Martin, C. R. *J. Electroanal. Chem.* **2002**, *522*, 66-69.

58 Kyotani, T.; Tsai, L.; Tomita, A. *Chem. Mater.* **1996**, *8*, 2109.

59 Yuan, Z. h.; Huang, H.; Liu, L.; Fan, S. S. *Chem. Phys. Lett.* **2001**, *345*, 39-43.

60 Kyotani, T.; Ma, Z.; Tomita, A. *Carbon* **2003**, *41*, 1451-1459.

61 Cepak, V. M.; Hulteen, J. C.; Che, G.; Jirage, K. B.; Lakshmi, B. B.; Fisher, E. R.; Martin, C. R.; Yoneyama, H. *Chem. Mater.* **1997**, *9*, 1065-1067.

62 Lakshmi, B. B , Martin, C R. *Proc -Electrochem Soc* **1997**, *97-11*, 47-55

63 Lakshmi, B. B , Patrissi, C. J ; Martin, C. R. *Chem. Mater* **1997**, *9*, 2544-2550

64 Mitchell, D T , Lee, S. B , Trofin, L., Li, N ; Nevanen, T K., Soederlund, H ; Martin, C R. *J Am. Chem Soc* **2002**, *124*, 11864-11865

65 Ikegame, M ; Tajima, K., Aida, T *Angew Chem.-Int Edit* **2003** *42*, 2154-2157.

66 Lei, J ; Cai, Z., Martin, C R. *Synth. Met* **1992**, *46*, 53-69

67 Parthasarathy, R. V , Martin, C R. *Chem. Mater* **1994**, *6*, 1627-1632

68 Joo, J , Park, K. T., Kim, B H., Kim, M. S , Lee, S. Y ; Jeong C K.; Lee, J K., Park, D H ; Yi, W K., Lee, S H.; Ryu, K. S *Synth. Met.* **2003**, *135-136*, 7-9

69 Tierney, M. J , Martin, C R. *J Phys Chem.* **1989**, *93*, 2878-2880

70 Nicewarner-pena, S R., Freeman, R. G ; Reiss, B D ; He, L , Pena, D J ; Walton, I D , Cromer, R., Keating, C. D , Natan, M. J. *Science* **2001**, *294*, 137-141

71 Hulteen, J C., Jirage, K. B ; Martin, C R. *J Am. Chem. Soc* **1998**, *120*, 6603-6604

72 Jirage, K. B , Hulteen, J. C., Martin, C R. *Science* **1997**, *278*, 655-658

73 Jirage, K. B , Hulteen, J. C , Martin, C. R. *Anal. Chem* **1999**, *71*, 4913-4918.

74 Kobayashi, Y ; Martin, C R. *J Electroanal. Chem.* **1997**, *431*, 29-33.

75 Kobayashi, Y ; Martin, C R. *Anal Chem.* **1999**, *71*, 3665-3672.

76 Petzny, W J ; Quinn, J A. *Science* **1969**, *166*, 751-753

77 Wirtz, M., Yu, S ; Martin, C R. *Analyst* **2002** *127*, 871-879

78 Martin, C R.; Nishizawa, M., Jirage, K., Kang M. *J Phys Chem. B* **2001**, *105*, 1925-1934

79 Lee, S B ; Martin, C R. *Anal Chem.* **2001**, *73*, 768-775

80 Lee, S B ; Martin, C R. *J Am. Chem. Soc.* **2002**, *124*, 11850-11851

81 Russel, A., Repka, K.; Dibble, T ; Ghoroghchian, J , Smith, J J ; Fleischman, M , Pitt, C H., Pons, S. *Anal Chem* **1986**, *58*, 2961.

82. Bond, A M , Henderson, T. L E., Mann, D R., Thormann, W., Zoski, C. G. *Anal Chem* **1988**, *60*, 1878

83 Wirtz, M , Martin, C R. *Adv Mater* **2003**, *15*, 455-458

84 Steinle, E D ; Mitchell, D T ; Wirtz, M , Lee, S B , Young, V Y , Martin, C. R. *Anal Chem.* **2002**, *74*, 2416-2422.

85 Bayley, H , Martin, C. R *Chem. Rev* **2000**, *100*, 2575-2594

86 Sapp, S A., Mitchell, D T , Martin, C R. *Chem. Mater* **1999**, *11*, 1183-1185

87 Ghosh, R., Cui, Z. F *J Membr Sci.* **2000** *167*, 47-53

88 Howell, J. A., Wu, D ; Field, R. W *J Membr Sci.* **1999**, *152*, 117-127

89 Li, Q Y , F , C Z., Pepper, D. S *J Membr Sci* **1997**, *136*

90 Guell, C , Davis, R. H *J Membr Sci.* **1996** *119*, 269-284

91 van Reis, R., Brake, J M., Charkoudian, J , Burns, D B., Zydney, A L *J Membr Sci.* **1999**, *159*, 133-142

92 Saksena, S , Zydney, A. L. *Biotechnol. Bioeng* **1994** *43*, 960-968

93 Van Eijndhoven, R. H. C M ; Saksena, S., Zydney, A. L *Biotechnol Bioeng* **1995** *48* 406-414

94 Shul R. J., Pearton, S J *Handbook of Advanced Plasma Processing Techniques*, Springer Berlin Heidelberg New York, 2000

95 Kuo, C -W , Shiu, J -Y , Cho, Y -H , Chen, P *Adv Mater* **2003** *15*, 1065-1068

96 Kuo, C.-W., Shiu, J.-Y., Chen, P *Chem Mater* **2003**, *15*, 2917-2920.

97 Hegemann, D., Brunner, H ; Oehr, C *Nuclear Instruments & Methods in Physics Research Section B Beam Interactions with Materials and Atoms* **2003**, *208*, 281-286

98 Iritani, E ; Mukai, Y , Murase, T *Filtration and Separation* **1997**, 967-973

99 Ghosh, R., Cui, Z. F *J Membr Sci.* **2000** *167*, 47-53

100 Ramamoorthy, M ; Raju, M D *Ind. Eng. Chem Res* **2001** *40*, 4815-4820

101 Ghosh, R., Cui, Z. F *J Membr Sci.* **1998**, *139*, 17-28

102 Ho, A K., Perera, J M., Dunstan, D E., Stevens, G W., Nystrom, M *AIChE J* **1999**, *45*, 1434-1450

103 D Connor, A. J , Pratt, H. R. C ; Stevens, G W *Chem. Eng. Sci* **1996** *51*, 3459-3477

104 Li, Q. Y., Pepper, D. S. *J. Membr. Sci.* **1997**, *136*, 181-190

105 Li, Q. Y., Ghosh, R., Bellara, S. R., Cui, Z. F., Pepper, D. S. *Separation and Purification Technology* **1998**, *14*, 79-83

106. Zydney, A. L. *Inter. Dairy J.* **1998**, *8*, 243-250

107 van Reis, R., Gadam, S., Frautschy, L. N., Orlando, S., Goodrich, E. M., Saksena, S., Kuriyel, R., Simpson, C. M., Pearl, S., Zydney, A. L. *Biotechnol. Bioeng.* **1997**, *56*, 71-82.

108. Nystrom, M., Aimar, P., Luque, S., Kulovaara, M., Metsamuuronen, S. *Colloids Surf. A* **1998**, *138*, 185-205

109. Ho, C., Zydney, A. L. *J. Membr. Sci.* **1999**, *155*, 261-275

110 Nakatsuka, S., Michaels, A. S. *J. Membr. Sci.* **1992**, *69*, 189-211

111. Guell, C., Davis, R. H. *J. Membr. Sci.* **1998**, *119*, 269-284

112. Mueller, J., Davis, R. H. *J. Membr. Sci.* **1996**, *116*, 47-60

113 Jones, K. L., O'Melia, C. R. *J. Membr. Sci.* **2000**, *165*, 31-46.

114 Kang, M.-S., Martin, C. R. *Langmuir* **2001**, *17*, 2753-2759

115 Hou, Z., Abbott, N. L., Stroeve, P. *Langmuir* **2000**, *16*, 2401-2404

116 Chun, K. Y., Stroeve, P. *Langmuir* **2002**, *18*, 4653-4658

117 Yu, S., Lee, S. B., Kang, M., Martin, C. R. *Nano Lett.* **2001**, *1*, 495-498

118 Yu, S., Lee, S. B., Martin, C. R. *Anal. Chem.* **2003**, *75*, 1239-1244

119 Howell, J. A., Wu, D., Field, R. W. *J. Membr. Sci.* **1999**, *152*, 117-127.

120 Zeman, L. J., Zydney, A. L. *Microfiltration and Ultrafiltration Principles and Applications*; Marcel Dekker: New York, 1996

121 Musale, D. A., Kulkarni, S. S. *J. Membr. Sci.* **1997**, *136*, 13-23

122 van Reis, R., Brake, J. M., Charkoudian, J., Burns, D. B., Zydney, A. L. *J. Membr. Sci.* **1999**, *159*, 133-142.

123 Kim, K. J., Fane, A. G., Nystroem, M., Pihlajamaki, A. *J. Membr. Sci.* **1997**, *134*, 199-208.

124. Lu, H. B., Campbell, C. T., Castner, D. G. *Langmuir* **2000**, *16*, 1711-1718

125 Harris, J. M. *Poly(ethylene Glycol) Chemistry: Biotechnical and Biomedical Applications*; Plenum Publishing: New York, 1992.

126 Malmsten, M.; Van Alstine, J. M. *J. Colloid Interface Sci.* **1996**, *177*, 502-512.

127 Emoto, K.; Van Alstine, J. M.; Harris, J. M. *Langmuir* **1998**, *14*, 2722-2729.

128 Prime, K. L.; Whitesides, G. M. *Science* **1991**, *252*, 1164-1167.

129 Harder, P.; Grunze, M.; Dahint, R.; Whitesides, G. M.; Laibinis, P. E. *J. Phys. Chem. B* **1998**, *102*, 426-436.

130 Bellara, S. R.; Cui, Z.; Pepper, D. S. *Biotech. Prog.* **1997**, *13*, 869-872.

131 Deen, W. M. *AIChE J.* **1987**, *33*, 1409-1425.

132 Freeman, B. D. *Macromolecules* **1999**, *32*, 375-380.

133 Miller, S. A.; Young, V. Y.; Martin, C. R. *J. Am. Chem. Soc.* **2001**, *123*, 12335-12342.

134 Rylatt, D. B.; Napoli, M.; Ogle, D.; Gilbert, A.; Lim, S.; Nair, C. H. *J. Chromatogr. A* **1999**, *865*, 145-153.

135 Anfinsen, C. B.; Edsall, J. T.; Richards, F. M. *Advances in Protein Chemistry*; Academic Press: Orlando, FL, 1985.

136 Hinz, H.-J. *Thermodynamic Data for Biochemistry and Biotechnology*; Springer: Berlin, 1986.

137 Martin, C. R. *Accounts Chem. Res.* **1995**, *28*, 61-68.

138 Patrissi, C. J.; Martin, C. R. *J. Electrochem. Soc.* **2001**, *148*, A1247-A1253.

139 Lee, S. B.; Mitchell, D. T.; Trofin, L.; Nevanen, T. K.; Soederlund, H.; Martin, C. R. *Science* **2002**, *296*, 2198-2200.

140 Duchet, J.; Legras, R.; Demoustier-Champagne, S. *Synth. Met.* **1998**, *98*, 113-122.

141 Schoenenberger, C.; van der Zande, B. M. I.; Fokkink, L. G. J.; Henny, M.; Schmid, C.; Krueger, M.; Bachtold, A.; Huber, R.; Birk, H.; Staufer, U. *J. Phys. Chem. B* **1997**, *101*, 5497-5505.

142 Kim, G. M.; van den Boogaart, M. A. F.; Brugger, J. *Microelectronic Engineering* **2003**, *67-68*, 609-614.

143 Xia, Y.; Rogers, J. A.; Paul, K. E.; Whitesides, G. M. *Chem. Rev.* **1999**, *99*, 1823-1848.

144 Michel, B , Bernard, A., Bietsch, A., Delamarche, E , Geissler, M., Juncker, D., Kind, H ; Renault, J P , Rothuizen, H., Schmid, H., Schmidt-Winkel, P ; Stutz, R., Wolf, H. *IBM J Res Develop* **2001**, *45*, 697-719

145 Kumar, A., Whitesides, G. M. *Appl Phys. Lett.* **1993**, *63*, 2002-2004

146 Xia, Y., Whitesides, G. M. *Angew Chem.-Inter Edit.* **1998**, *37*, 550-575.

147 Pantano, P , Walt, D R. *Chem Mater* **1996** *8*, 2832-2835.

148 Magonov, S N *Surface Analysis with STM and AFM*, Weinheim New York, 1996

149 Noy, A., Vezenov, D V , Lieber, C. M *Annu. Rev Mater Sci.* **1997**, *27*, 381

150 Binnig, G ; Quate, C F , Gerber, C *Phys Rev Lett* **1986**, *56*, 930-933

151 Gavoille, J ; Takadoum, J *Tribology International* **2003**, *36*, 865-871

152 Li, N , Mitchell, D T ; Lee, K. P ; Martin, C R. *J Electrochem. Soc* **2003**, *150*, A979-A984.

153 Stoeber, W , Fink, A., Bohn, E. *J Colloid Interface Sci* **1968**, *26*, 62-69.

154 Qhobosheane, M S., Zhang, P and Tan, W. *Analyst* **2001**, *126*, 1274-1278

155 He, X.-X , Wang, K ; Tan, W , Liu, B , Lin, X , He, C., Li, D , Huang, S , Li, J *J Am Chem Soc* **2003** *125*, 7168-7169

156 Green, J.-B D , McDermott, M T , Porter, M D , Siperko, L M. *J Phys. Chem.* **1995**, *99*, 10965-10970

BIOGRAPHICAL SKETCH

Shufang Yu was born in Qingdao, China. She spent 4 years at Qingdao University earning a B.S. in chemistry in 1993. After graduation, she was a teaching specialist in Qingdao University for three years. She completed an M.S. in polymer chemistry and physics at the University of Science and Technology of China (USTC) in 1999. In August 1999, Shufang entered graduate school in the Chemistry Department at the University of Florida under the guidance of Dr. Charles R. Martin. She completed her research in December 2003, obtaining a Doctor of Philosophy degree.

I certify that I have read this study and that in my opinion it conforms to acceptable standards of scholarly presentation and is fully adequate, in scope and quality, as a dissertation for the degree of Doctor of Philosophy

Charles R. Martin, Chairman
Professor of Chemistry

I certify that I have read this study and that in my opinion it conforms to acceptable standards of scholarly presentation and is fully adequate, in scope and quality, as a dissertation for the degree of Doctor of Philosophy

James D. Winefordner
Graduate Research Professor of Chemistry

I certify that I have read this study and that in my opinion it conforms to acceptable standards of scholarly presentation and is fully adequate, in scope and quality, as a dissertation for the degree of Doctor of Philosophy

James A. Deyrup
Professor of Chemistry

I certify that I have read this study and that in my opinion it conforms to acceptable standards of scholarly presentation and is fully adequate, in scope and quality, as a dissertation for the degree of Doctor of Philosophy

Anna Brajter Toth
Associate Professor of Chemistry

I certify that I have read this study and that in my opinion it conforms to acceptable standards of scholarly presentation and is fully adequate, in scope and quality, as a dissertation for the degree of Doctor of Philosophy

Wolfgang M. Sigmund
Associate Professor of Materials Science and Engineering

This dissertation was submitted to the Graduate Faculty of the Department of Chemistry in the College of Liberal Arts and Sciences and to the Graduate School and was accepted as partial fulfillment of the requirements for the degree of Doctor of Philosophy

December, 2003

Dean, Graduate School